ILMATIETEEN LAITOS
METEOROLOGISKA INSTITUTET
FINNISH METEOROLOGICAL INSTITUTE

RAPORTTEJA
RAPPORTER
REPORTS
2016:7

DEVELOPMENT OF CLIMATE CHANGE SCENARIOS FOR LATVIA FOR THE PERIOD UNTIL THE YEAR 2100

KIMMO RUOSTEENOJA
MATTI KÄMÄRÄINEN
SVETLANA AŅISKEVIČA
PENTTI PIRINEN
ANTTI MÄKELÄ

WWW.FMI.FI

RAPORTTEJA
RAPPORTER
REPORTS
No. 2016:7

551.583, 551.581.1, 551.588.7

Development of climate change scenarios for Latvia for the period until the year 2100

Kimmo Ruosteenoja[1]
Matti Kämäräinen[1]
Svetlana Aņiskeviča[2]
Pentti Pirinen[1]
Antti Mäkelä[1]

[1] **Finnish Meteorological Institute**
[2] **Latvian Environment, Geology and Meteorology Centre**

Ilmatieteen laitos
Meteorologiska Institutet
Finnish Meteorological Institute

Helsinki 2016

ISBN 978-952-336-003-7 (pdf)

ISSN 0782-6079

Helsinki 2016

FINNISH METEOROLOGICAL INSTITUTE

Published by	Finnish Meteorological Institute (Erik Palménin aukio 1) , P.O. Box 503 FIN-00101 Helsinki, Finland	Series title, number and report code of publication Reports 2016:7 Date 2016
Author(s)	Kimmo Ruosteenoja, Matti Kämäräinen, Svetlana Aņiskeviča, Pentti Pirinen and Antti Mäkelä	Name of project Climate change scenario development for Latvia Commissioned by Latvian Environment, Geology and Meteorology Centre (LEGMC)

Title Development of climate change scenarios for Latvia for the period until the year 2100

Abstract

This report examines climatic changes projected for Latvia during the 21st century. Climate projections are based on a wide ensemble of state-of-the-art CMIP5 global climate models; that set of models was utilized in compiling the 5th Assessment Report of the Intergovernmental Panel on Climate Change. Projections have been elaborated separately for three greenhouse gas scenarios, the RCP2.6 scenario representing small, RCP4.5 medium and RCP8.5 large emissions.

By the late 21st century, the following changes (expressed relative to the mean of the period 1971-2000) are projected:

• In winter, mean temperatures are projected to increase by 1-4 °C under RCP2.6, 2-6 °C under RCP4.5 and 4-9 °C under RCP8.5. In summer, anticipated warming is weaker: 1-3 °C under RCP2.6, 1-4 °C under RCP4.5 and 2-7 °C under RCP8.5. In winter, warming appears to be somewhat larger in the eastern part of the country while in summer the geographical differences are small.

• Diurnal temperature range would diminish in winter by 0-50 % and incident solar radiation by 0-30 %. In summer, changes in these quantities are most likely positive but fairly small.

• Mean winter precipitation increases by 0-20 % under RCP2.6, 0-30 % under RCP4.5 and 10-50 % under RCP8.5. In summer, the sign of change is uncertain, but in southern Latvia it is somewhat more likely that precipitation decreases slightly rather than increases.

• Ice days (with a maximum temperature below zero) become substantially less frequent while the count of summer days (maximum temperature above 25 °C) increases.

• Thermal growing season would lengthen by up to two months and the degree day sum would nearly double (under RCP8.5).

• According to the best estimate (multi-model mean), wind speeds would remain nearly unchanged throughout the year. Even so, scatter among the individual model projections is large, and in winter even changes larger than ± 20% are possible.

When studying projections for a less distant future, the sign of change is the same as what is projected for the late 21st century but the magnitude is smaller. The above uncertainty intervals of projected changes reflect mainly the inter-model differences but the contribution of natural unforced variability has also been taken into account.

In the course of the project, several data files have been delivered into Latvia to be used for additional analyses. These files include, for instance, the time series of 30-year running monthly mean changes and bias-corrected daily model output, both given for five climate variables and represented on a 10 x 10 km grid.

Publishing unit Climate centre (IKE)		
Classification (UDC) 551.583, 551.581.1, 551.588.7	Keywords climatic change, CMIP5 climate models, human influence on climate, RCP scenarios, bias correction	
ISSN and series title 0782-6079 Reports		
ISBN 978-952-336-003-7 (pdf)	Language English	Pages 51

ILMATIETEEN LAITOS

Julkaisun sarja, numero ja raporttikoodi
Raportteja 2016:7

Julkaisija	Ilmatieteen laitos, (Erik Palménin aukio 1) PL 503, 00101 Helsinki	Julkaisuaika	2016
Tekijä(t)	Kimmo Ruosteenoja, Matti Kämäräinen, Svetlana Aņiskeviča, Pentti Pirinen ja Antti Mäkelä	Toimeksiantaja	Latvian Environment, Geology and Meteorology Centre (LEGMC)
Nimike	Vuoteen 2100 saakka ulottuvat Latvian ilmastonmuutosskenaariot		

Tiivistelmä

Raportissa esitetään maailmanlaajuisiin CMIP5-ilmastomalleihin perustuvia arvioita Latvian ilmaston muuttumisesta tämän vuosisadan aikana. Näitä samoja malleja on käytetty myös Hallitustenvälisen Ilmastonmuutospaneelin viidettä arviointiraporttia laadittaessa. Latvian ilmastonmuutosennusteet on muodostettu erikseen kolmelle vaihtoehtoiselle kasvihuonekaasuskenaariolle, joista RCP2.6-skenaario edustaa varsin pieniä, RCP4.5 kohtalaisia ja RCP8.5 hyvin suuria kasvihuonekaasujen päästöjä. Ilmastoennusteita esitettäessä vertailukohtana käytetään jakson 1971-2000 keskimääräistä ilmastoa.

Tämän vuosisadan loppua lähestyttäessä (jakso 2070-2099) Latvian ilmaston ennustetaan muuttuvan seuraavankaltaisesti:

• Talven keskilämpötilojen arvioidaan nousevan RCP2.6-skenaarion mukaan 1-4°C, RCP4.5 skenaarion mukaan 2-6°C ja RCP8.5-skenaarion toteutuessa 4-9°C. Kesällä lämpötilat näyttävät kohoavan vähemmän: 1-3°C (RCP2.6), 1-4°C (RCP4.5) tai 2-7°C (RCP8.5). Talvisin lämpiäminen on jonkin verran voimakkaampaa Latvian itä- kuin länsiosissa, kun taas kesällä erot maan eri osien välillä ovat pieniä.

• Lämpötilan vuorokaudensisäisten vaihtelujen ennustetaan vaimentuvan talvisin 0-50 % ja maanpinnalle saapuvan auringonsäteilyn vähentyvän 0-30 %. Kesällä vuorokautiset lämpötilanvaihtelut ja auringonsäteily taas näyttäisivät aavistuksen lisääntyvän.

• Sademäärä kasvaa talvella RCP2.6-skenaarion mukaan 0-20 %, RCP4.5:n perusteella 0-30 % ja RCP8.5-skenaarion toteutuessa 10-50 %. Kesällä sademäärän muutoksen suuntaa ei voida varmasti sanoa, mutta Etelä-Latviassa sateet mahdollisesti vähenevät jonkin verran.

• Jääpäivät, jolloin lämpötila pysyy koko vuorokauden pakkasen puolella, käyvät tulevaisuudessa selvästi harvinaisemmiksi. Vastaavasti hellepäivien (ylin lämpötila > 25°C) määrä kasvaa huomattavasti.

• RCP8.5-skenaarion toteutuessa terminen kasvukausi pidentyisi jopa kahdella kuukaudella ja kasvukauden tehoisa lämpösumma lähes kaksinkertaistuisi.

• Kun tarkastellaan kaikkien mallien ennustamien muutosten keskiarvoa, tuulen nopeudet näyttävät säilyvän varsin tarkkaan ennallaan ympäri vuoden. Eri mallien tulokset poikkeavat kuitenkin toisistaan paljon, ja talvella jopa yli 20 % muutokset suuntaan tai toiseen ovat mahdollisia.

Lähivuosikymmeninä ja vuosisadan puolivälissä muutoksen ovat samansuuntaisia mutta heikompia kuin mitä ennakoidaan koettavan vuosisadan lopulla. Muutosarvioitten epävarmuus aiheutuu ensisijaisesti eri mallien välisistä eroista, mutta myös ilmaston luonnollinen vaihtelu tuo siihen oman lisänsä.

Tämän hankkeen päätyttyä latvialaiset jatkavat ilmastonmuutosten tutkimista omatoimisesti, ja tätä varten heille on toimitettu joukko mallituloksiin perustuvia tiedostoja: esimerkiksi muutosten kuukausikeskiarvot 30-vuotisina liukuvina keskiarvoina sekä harhasta korjattuja malliajojen päivittäisiä tulostietoja. Nämä tiedot on interpoloitu Latvian kattavaan 10 km x 10 km hilaan.

Julkaisijayksikkö Ilmastokeskus (IKE)		
Luokitus (UDK) 551.583, 551.581.1, 551.588.7	Asiasanat ilmastonmuutos, CMIP5-ilmastomallit, ihmiskunnan vaikutus ilmastoon, RCP-skenaariot, harhankorjaus	
ISSN ja avainnimike 0782-6079 Raportteja		
ISBN 978-952-336-003-7 (pdf)	Kieli Englanti	Sivumäärä 51

Contents

1 Introduction

According to IPCC (2013), global warming will continue during the 21st century, although the severity of the simulated changes varies among the climate models and is largely dependent on the evolution of future greenhouse gas emissions. The aim of the present project is to assess how this global-scale climatic change is reflected in the Latvian climate.

The present project has been financed through the project "Development of Proposal for National Adaptation Strategy, Including Identification of Scientific Data, Measures for Adapting to Changing Climate, Impact and Cost Evaluation", supported by the European Economic Area Financial Mechanism and implemented by the Latvian Environment, Geology and Meteorology Centre (LEGMC). Within the framework of this programme, LEGMC produces an analysis of long term observational climate data and develops climate change scenarios for the country. In this programme, the Finnish Meteorological Institute (FMI) was selected as a partner that provides model-based climate scenario data for the Latvian territory.

A reasonable general view on the projected climate change in Latvia can be obtained by studying the spatial averages over the country. This is due to the fairly small size of the country (about 400 x 200 km) compared to the typical horizontal scale of modelled changes in temperature, precipitation and other climate variables (Figs. 21–25 in this report; see also Fig. 12.10 of IPCC (2013)). Moreover, the topography of Latvia is gentle, with the majority of the country having a height of less than 200 m above the sea level, the coastline is fairly regular, and no archipelago or large lakes exist. Consequently, differences across the various climate model simulations tend to be much larger than the geographical differences of the projected changes within the country. Nonetheless, in addition to the spatial means, this report presents the geographical distribution of changes for the main climate variables.

In recent years, climate change scenarios have been created for several northern European countries, e.g., for Russia (Meleshko et al., 2008), Sweden (Lind and Kjellström, 2008), Estonia (Jaagus and Mändla, 2014) and Finland (Jylhä et al., 2009; Ruosteenoja et al., 2013). Moreover, climate scenario data have been distributed through the Finnish climate portal (climateguide.fi), for instance.

In the present project, climate scenarios have been derived from the output of global climate models (GCMs) participating in Phase 5 of the Coupled Model Intercomparison Project (CMIP5). This is the most recent comprehensive climate model ensemble available and has been utilized in compiling the climate projections presented in the 5th assessment report of the Intergovernmental Panel on Climate Change (IPCC). Projections are given separately for three greenhouse gas scenarios, one representing moderate, one medium and one strong climate change. The climate variables considered are daily mean, minimum and maximum temperature, precipitation and wind speed. In addition, some nationally-averaged projections are given for surface air pressure, incident solar radiation, and the length and degree days of the thermal growing season.

For the spatially-averaged projections, annual, seasonal and monthly means are presented for the three greenhouse gas scenarios, and for each scenario, the best estimates (multi-model means) and uncertainty assessments derived from the inter-model scatter are given. Seasonal and annual mean changes are presented in a tabular form as well: multi-model mean changes with 90 % uncertainty intervals and projected changes simulated by the individual GCMs.

In order to explore the geographical distributions, projected monthly changes have been interpolated onto a 10 x 10 km grid. These files have been delivered to LEGMC in Latvia and also used to compile maps of projected changes (Figs. 21–25).

The final task in the present project was to create a database that can be used in calculating diverse climate indices. For that purpose, files containing bias-corrected model output on the 10 x 10 km grid have been produced for selected GCMs. Bias correction requires fine-scale gridded daily observations that have been created at LEGMC by using a Kriging interpolation algorithm developed by FMI; an evaluation of these observation-based analyses is included in this report. To facilitate utilization of this database, we have calculated two example climate indices that can be used for comparison.

2 Production of the climate scenario data

2.1 Greenhouse gas scenarios

In the GCM runs that have been utilized in elaborating the present climate projections, the future evolutions of the greenhouse gas (carbon dioxide, methane, etc.) and aerosol particle concentrations have been represented with three alternative forcing scenarios called Representative Concentration Pathways or RCPs (van Vuuren et al., 2011). The time series of the emissions and atmospheric concentrations of the most important anthropogenic greenhouse gas, carbon dioxide, under the RCP scenarios are shown in Fig. 1. Under the RCP8.5 scenario[1], emissions continue to increase throughout the 21st century, ultimately nearly three-folding compared to the level that prevailed in 2000, and the concentration of CO_2 would approach 1000 ppm by 2100. According to the other two RCP scenarios, global emissions decline during this century. If the RCP4.5 scenario is realized, the CO_2 concentration stabilizes close to 540 ppm by the end of the century, i.e., at a level about double of that in the pre-industrial era. Under the low-emission RCP2.6 scenario, the concentrations start to diminish already after mid-century.

According to the present GCM simulations (section 2.2), all three greenhouse gas scenarios lead to an increase in global-mean temperature during the next few decades, but in the mid- and, in particular, late 21st century the global mean temperature projections diverge significantly among the scenarios (Fig. 2). If the emissions increase unabatedly (the RCP8.5 scenario), global warming even accelerates in the course of the century, and, by the late 21st century, global mean temperature may have increased by $\sim$4°C compared to the 1971–2000 mean, and even more relative to the pre-industrial level. Curtailing the emissions leads to a deceleration of global warming, and under the RCP2.6 scenario, global mean temperature would stabilize after mid-century.

In the present project, the RCP2.6 scenario stands for moderate, RCP4.5 for medium and RCP8.5 for significant climate change.

It should be noticed that the global-mean warming estimates depicted in Fig. 2 are subject to significant inter-model scatter. The importance of inter-model differences for the Latvian climate projections will be illustrated in Figs. 11–18.

[1]The label after the acronym RCP refers to the total radiative forcing (in Wm^{-2}) near the year 2100.

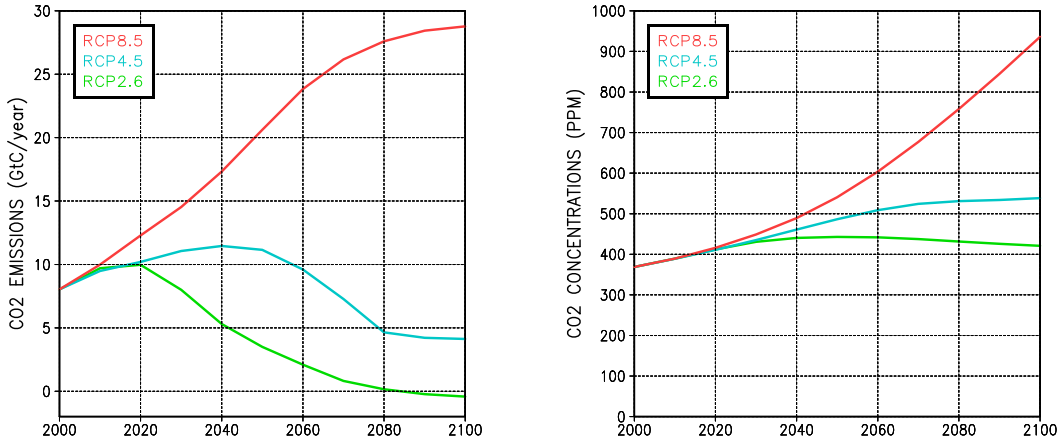

Figure 1. Temporal evolution of the global emissions (gigatonnes of carbon per year; left panel) and atmospheric concentrations (parts per million in volume (ppm); right panel) of carbon dioxide in 2000–2100 according to three RCP scenarios; see the legend.

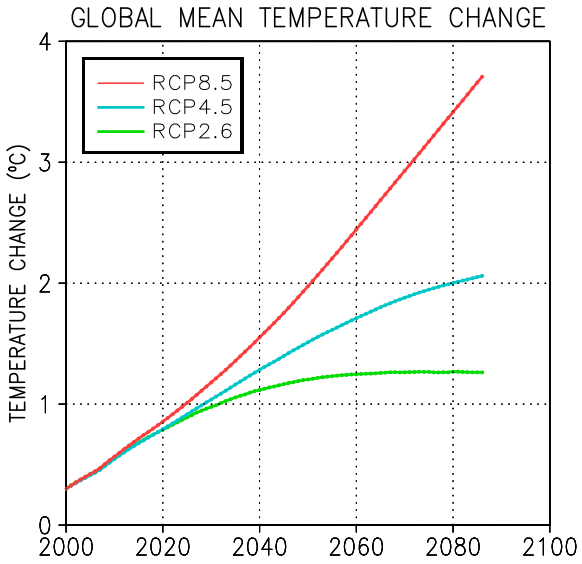

Figure 2. Projected changes in global mean surface air temperature (in °C) during the 21st century (30 year running means), relative to the mean of the baseline period 1971–2000; a mean of the simulations performed with the 28 GCMs listed in Table 1. Projections are depicted separately for three greenhouse gas scenarios: RCP8.5, RCP4.5 and RCP2.6 (see the legend). To obtain the temperature increase relative to the pre-industrial era, these estimates have to be elevated by about 0.5 °C due to the global warming that has occurred before the late 20th century.

2.2 Climate model data

The global climate models analyzed in this project are listed in Table 1. Further information about the individual GCMs, including the official references, can be seen in Table 9.A.1 of IPCC (2013).

Originally, we examined 35 GCMs but, as discussed in Luomaranta et al. (2014), seven of those models were excluded from the analysis. These rejected GCMs either failed to reproduce the recent past climate in Europe, gave severely biased simulated temperature trends during the instrumental period, or produced future temperature responses to the various RCP scenarios that were not mutually consistent. Accordingly, 28 models were used in calculating projections for surface air temperature and precipitation (as well as for surface air pressure and solar radiation, for which some spatial-mean results will also be presented) under RCP4.5 and RCP8.5 (Table 1). For the RCP2.6 scenario, data was provided by 21 models. In order to make the future projections mutually comparable for all three RCP scenarios, these missing GCM runs were replaced by surrogate data produced by a pattern-scaling technique (Ruosteenoja et al., 2007). This scaling procedure only influences the projections for the RCP2.6 scenario.

For daily maximum and minimum temperatures and wind speeds, data were lacking from a few GCMs. Moreover, in both versions of the IPSL model, diurnal temperature range proved to be unrealistically large, and therefore these models were not considered when studying the daily temperature minima and maxima. Consequently, 25 climate models were examined for the diurnal temperature cycle and 24 models for wind speed (for RCP4.5 and 8.5).

Many GCMs provide multiple parallel runs for the individual RCP scenarios, the maximum count of these runs being six (Table 1). Parallel runs are forced by identical greenhouse gas and aerosol concentrations, but the initial conditions in the runs diverge. Availability of several parallel runs helps to assess the component of uncertainty induced by unforced internal variability in the climate system (see below). In this report, changes in the temperature variables, precipitation, wind speed, etc. are means of all the parallel runs available for each GCM. On the other hand, bias-corrected data (section 2.7) will be given merely for the first parallel run. Accordingly, climate indices (section 2.8) are calculated for a single parallel run as well.

The computational grid varies among the 28 climate models. Therefore, in calculating the multi-model statistics, all model data were first interpolated bi-linearly onto a common 2.5 x 2.5 degree latitude-longitude grid. Spatial averages over Latvia were calculated as an area-weighted mean of those three grid points that fall within the territory of the country.

The future projections are expressed as changes relative to the means of the baseline period 1971–2000. Some GCM runs end in 2099, and therefore projections for the period 2071–2100 have been extrapolated from the 30-year means representing the periods 2069–2098 and 2070–2099.

In calculating the multi-model means and standard deviations for the simulated changes, all 28 GCMs were weighted equally, with the exception that no individual research centre was given more than two votes. Accordingly, halved weight coefficients were given for MIROC-ESM, MIROC-ESM-CHEM, CESM1-CAM5 and CESM1-BGC, while the remaining GCMs were weighted by unity.

For any individual RCP scenario, the uncertainty of future changes in a climate variable (e.g., temperature) consists of two components, modelling uncertainty and internal natural variability.

Table 1. Global climate models used in creating climate projections for Latvia. The first and second columns state the model acronym and the country of origin; the EC-EARTH model has been developed by a consortium of several European countries. Columns 3–5 give, for each RCP scenario, the number of parallel runs for temperature and precipitation simulations (for the other variables, the number of runs is different for some models). Finally, there is a list of variables for which data have been analyzed in the present work for each individual model (T: surface air temperature; PR: precipitation; TXN: daily maximum and minimum temperatures; W: surface air wind speed).

Model	Country	$N_{2.6}$	$N_{4.5}$	$N_{8.5}$	Variables
MIROC5	Japan	3	3	3	T, PR, TXN, W
MIROC-ESM	Japan	1	1	1	T, PR, TXN, W
MIROC-ESM-CHEM	Japan	1	1	1	T, PR, TXN, W
MRI-CGCM3	Japan	1	1	1	T, PR, TXN, W
BCC-CSM1-1	China	1	1	1	T, PR, TXN, W
INMCM4	Russia	-	1	1	T, PR, TXN, W
NorESM1-M	Norway	1	1	1	T, PR, TXN
NorESM1-ME	Norway	1	1	1	T, PR
HadGEM2-ES	U.K.	4	4	4	T, PR, TXN, W
HadGEM2-CC	U.K.	-	1	3	T, PR, TXN, W
MPI-ESM-LR	Germany	3	3	3	T, PR, TXN, W
MPI-ESM-MR	Germany	1	3	1	T, PR, TXN, W
CNRM-CM5	France	1	1	5	T, PR, TXN, W
IPSL-CM5A-LR	France	4	4	4	T, PR, W
IPSL-CM5A-MR	France	1	1	1	T, PR, W
CMCC-CM	Italy	-	1	1	T, PR, TXN, W
CMCC-CMS	Italy	-	1	1	T, PR, TXN, W
GFDL-CM3	U.S.A.	1	1	1	T, PR, TXN, W
GFDL-ESM2M	U.S.A.	1	1	1	T, PR, TXN, W
GISS-E2-R	U.S.A.	1	5	1	T, PR, TXN, W
GISS-E2-H	U.S.A.	1	5	1	T, PR, TXN, W
NCAR-CCSM4	U.S.A.	5	6	6	T, PR, TXN
NCAR-CESM1-CAM5	U.S.A.	3	3	3	T, PR, TXN, W
NCAR-CESM1-BGC	U.S.A.	-	1	1	T, PR, TXN
CanESM2	Canada	5	5	5	T, PR, TXN, W
ACCESS1-0	Australia	-	1	1	T, PR, TXN, W
ACCESS1-3	Australia	-	1	1	T, PR, TXN, W
EC-EARTH	Europe	2	6	6	T, PR, TXN, W

Ruosteenoja et al. (2016) derived equations that can be used to obtain the total variance of uncertainty as a sum of these two components. This can be done by inspecting the parallel run mean changes and deviations thereof.

After calculating the standard deviations of the total projection uncertainty, 90 % uncertainty intervals for the change were calculated by using the normality approximation (multimodel mean change ± 1.645 times the standard deviation of the simulated changes).

2.3 Projections for the thermal growing season

Thermal growing season is defined as that part of the year when daily mean temperature exceeds the +5°C threshold value. The growing degree day sum (also called 'temperature sum' or 'temperature accumulation') is calculated by summing the temperature excesses above that threshold over the growing season.

Projections for the onset and termination dates of the thermal growing season, based on simulations of 22–23 climate models, are available for the RCP4.5 and RCP8.5 scenarios (Ruosteenoja et al., 2016). Moreover, that paper deals with projections for the growing degree day sum for both scenarios.

In this report, the growing season data are given for a grid point in central Latvia.

2.4 Monthly mean climate change projections on a 10 km grid covering Latvia

To assess the horizontal distribution of the responses, projected multi-model mean changes in the daily mean, minimum and maximum temperatures, precipitation and scalar wind velocity were interpolated onto the 10 x 10 km LKS92 grid covering Latvia. Overlapping 30-year running means were given for the periods from 1960–1979 to 2071–2100. Again, changes are presented relative to the mean of the baseline period (1971–2000). Note that, in addition to the projection periods from 2010–2039 to 2071–2100, these time series include model-estimated changes for the periods from 1960–1979 onwards, so that the users of the data have an opportunity to compare recent modelled trends in the various climate variables with their observed counterparts.

Projections for the temperature variables were given in °C, changes in precipitation and wind velocity in per cent. The projections are based on simulated changes averaged over the 28 climate models (and on a slightly smaller number of GCMs for Tmin, Tmax and wind speed, see Table 1) and are given separately for the three greenhouse-gas scenarios (RCP2.6, RCP4.5 and RCP8.5) and all 12 calendar months. The time series were provided in the form of csv data files. Some example figures are displayed later in this report (Figs. 21–25).

2.5 Guidance: how to produce projections in absolute terms

The procurement only obliged FMI to provide climate **change** scenarios. However, projections for the climate variables are often needed in absolute terms as well. For this purpose, the generally-used **delta-change** approach can be applied. To obtain mean temperatures for the

future, the projected monthly mean temperature changes are directly added to the corresponding observational mean temperatures of the period 1971–2000. Daily minimum and maximum temperatures are treated analogously.

Correspondingly, precipitation projections can be produced by multiplying the observation-based monthly mean precipitation in 1971–2000 by the factor 1 + DP/100, where DP stands for the projected percentual change in precipitation. In principle, a similar procedure can be applied to percentual wind speed projections. One should note, however, that the observation-based gridded datasets for wind are rather unreliable, since wind speeds are strongly dependent on local micro-meteorological conditions near the observation sites.

2.6 Observational data on the 10 x 10 km grid

For correcting biases in the model-produced time series of the various climate quantities (section 2.7), one needs gridded observation-based time series for the respective variables. These daily time series for the period 1961–2010 (for wind speed, from 1966 onwards), represented on the 10 x 10 km LKS92 grid covering Latvia, have been produced by using the Kriging interpolation method. For that purpose, a modified version of the interpolation algorithm developed at FMI (Aalto et al., 2016) was used. In generating the analyses for Finland with the same algorithm, observations from selected sites outside the Finnish territory were included, in addition to a wide set of domestic observations. For Latvia, however, the option of including observations from the neighbouring countries was not utilized.

In Figs. 3–6, the long-term monthly means of four climate quantities (daily mean, minimum and maximum temperatures and precipitation) produced by the Kriging interpolation are compared with their counterparts derived from the E-OBS analyses (version 12.0) covering the entire European continent (Haylock et al., 2008). The E-OBS analyses have been represented on a 0.25 x 0.25 degree grid, and therefore, before calculating the differences, the Kriging products have been interpolated onto the same grid.

In the monthly mean temperatures (Fig. 3), differences between the two datasets are generally fairly modest, on the order of magnitude of 0.0–0.4 °C. Larger differences (∼0.4–0.8 °C) occur in the southeastern corner of Latvia near the Belarussian border (in winter and late spring) and near the eastern coast of Gulf of Riga close to the Estonian border (in summer), for instance. For daily maximum and minimum temperatures, areas with a substantial difference tend to be far wider (Figs. 4–5).

Large local differences between the two observation-based datasets near the borders of the country are presumably caused by the application of the Kriging algorithm. By definition, the outcome of the interpolation is typically not realistic close to the boundaries of the domain. This problem would have been eluded by including observations from the neighbouring countries in the analysis, but, as mentioned above, this alternative was not applied here.

In the daily minima and maxima in particular, differences between the two analyses also reflect spatial variations in the surface topography. For example, in the Vidzeme upland area near 57°N, 26°E, there are systematically lower temperature minima (throughout the year) and higher maxima (in spring and early summer) in the Kriging product compared to the E-OBS analyses. Such differences are likely to be due to the more dense observation network utilized in the Kriging analysis. For example, observation from Zoseni, one of the highest observation sites in

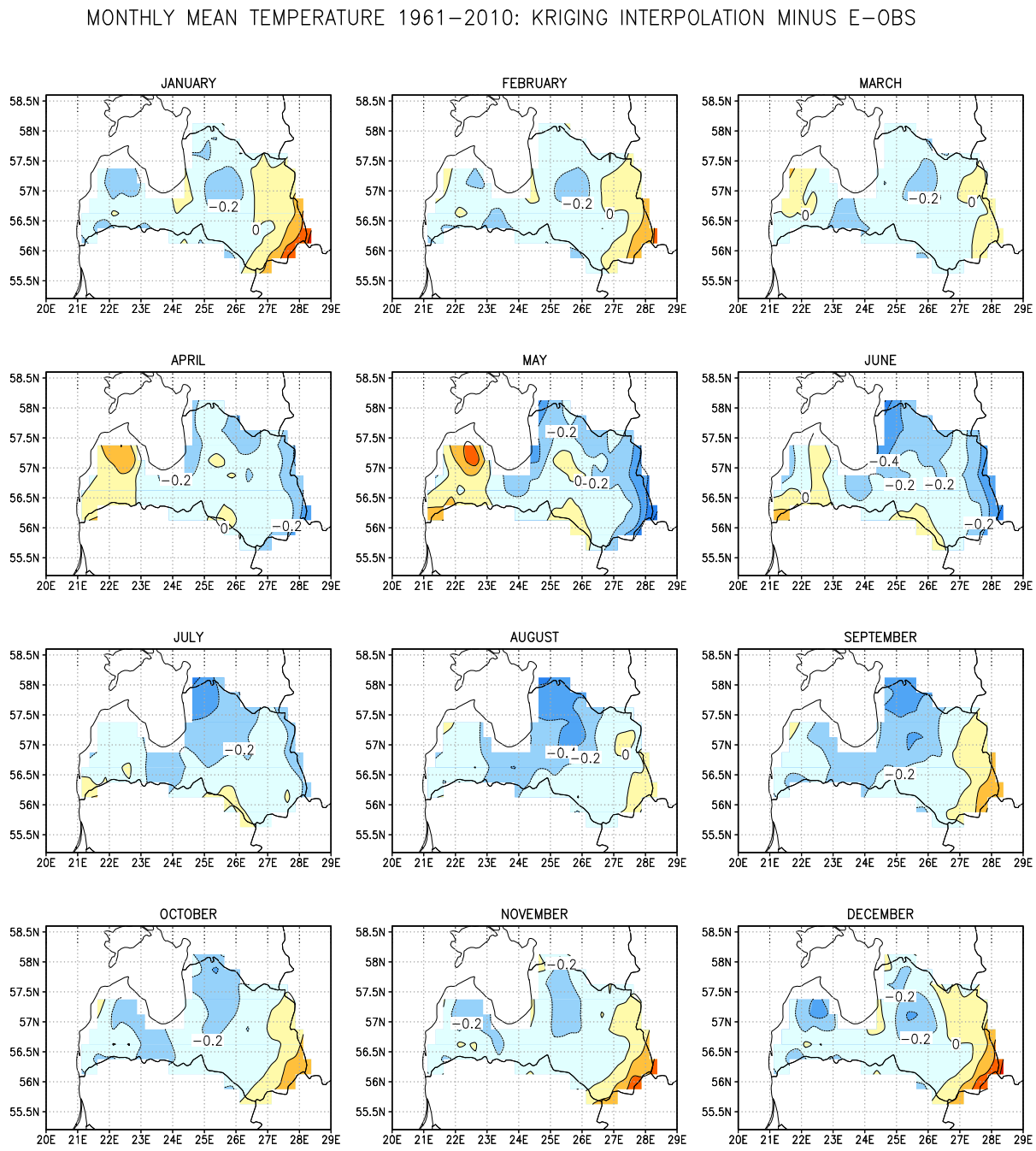

Figure 3. Climatological monthly mean temperatures for the period 1961–2010: the differences between monthly means derived from data interpolated onto the 10 x 10 km grid using Kriging and from the E-OBS analyses. Contour interval 0.2°C.

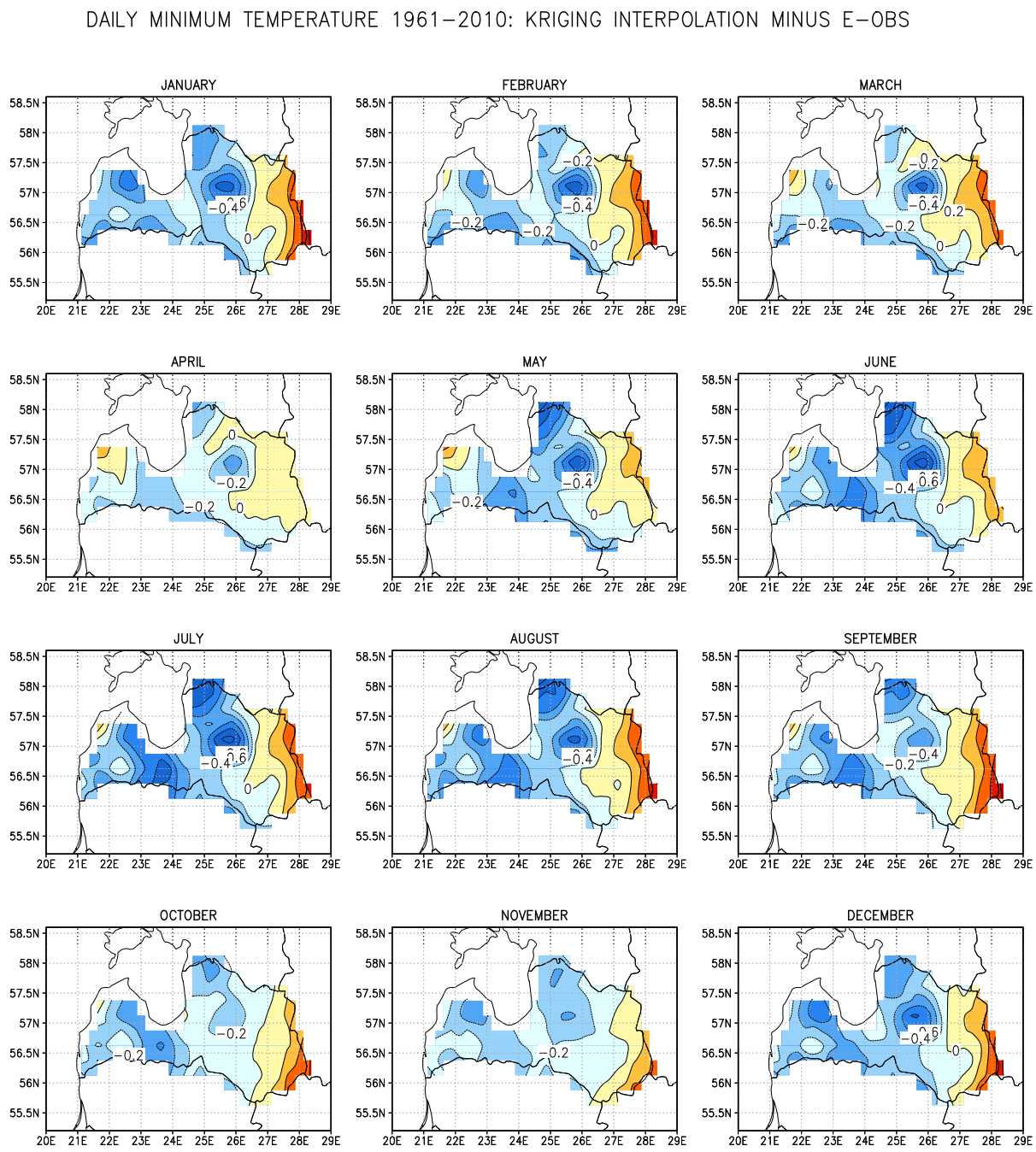

Figure 4. As in Fig. 3, but for the daily minimum temperatures. Contour interval 0.2°C.

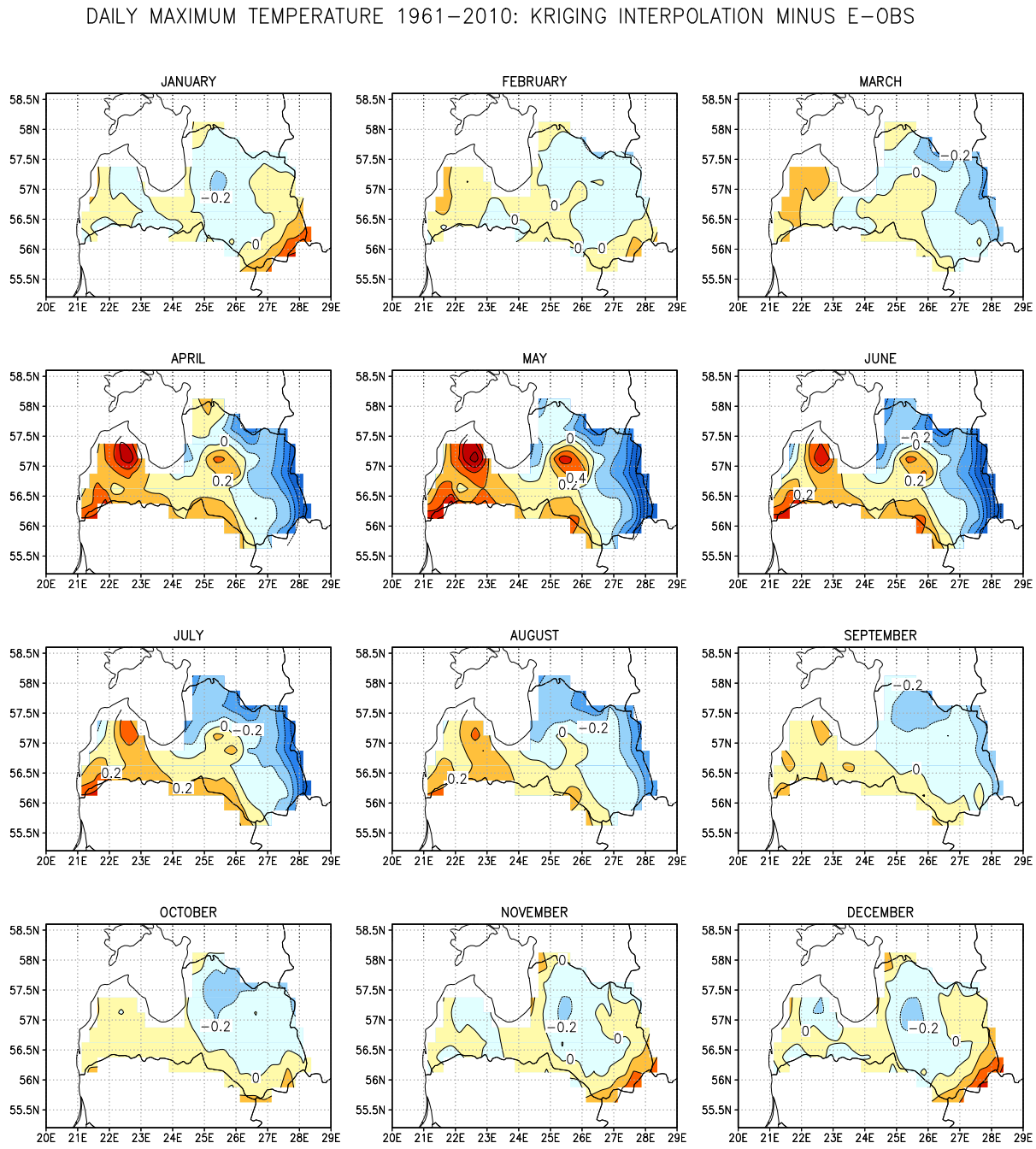

Figure 5. As in Fig. 3, but for the daily maximum temperatures. Contour interval 0.2°C.

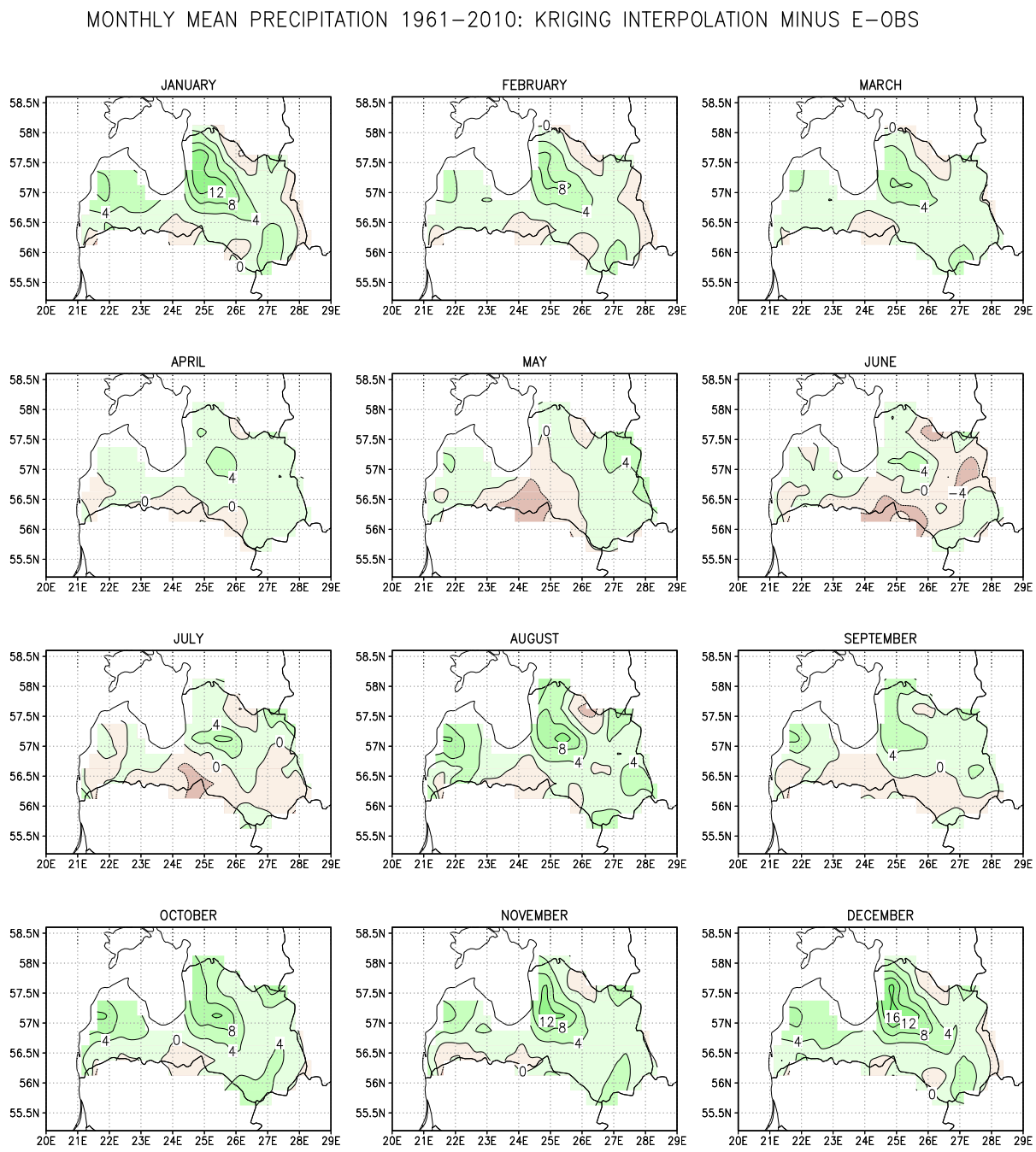

Figure 6. As in Fig. 3, but for mean precipitation totals. Contour interval 4 mm/month.

Latvia with an elevation of 187 m above the sea level, were not included in creating the E-OBS dataset but were utilized in elaborating the Kriging analyses.

Still, it is also possible that the above-mentioned differences might partly be an artefact induced by the Kriging interpolation procedure. When there are only a few high-topography observation sites in the observational dataset, the local microclimate at these stations may influence the outcome of the interpolation. For example, if these high-lying stations happen to reside in valleys, where daily temperature maxima are high and minima low, the Kriging algorithm then imagines that the diurnal temperature range should be generally wide in elevated areas.

For precipitation, differences in the monthly means derived from the Kriging and E-OBS products are substantial, up to $\geq$ 10 mm/month (Fig. 6). In the bulk of the domain, the Kriging product is wetter than its E-OBS-derived counterpart. In particular, the Kriging analyses yield large precipitation totals for an area located to the east-northeast of Riga in autumn and winter. There are two precipitation-rich stations (Limbazi and Sigulda) in this area, from which data were included in the Kriging but not in the E-OBS analysis. This may largely explain differences between the analyses in this area. In precipitation, no particularly striking method-induced differences are seen near the boundaries. Some stations from which data were employed in the Kriging analyses of precipitation reside quite close to the border of Latvia. Moreover, possible artefacts caused by the boundaries of the domain may be hidden by the fairly large differences existing everywhere over the domain.

Analyses of wind speed are not included in the E-OBS data archive, and therefore any quantitative evaluation of the Kriging output was not possible. Nonetheless, caution is recommended in using the interpolated winds as well, especially close to the boundaries of the country.

2.7 Bias correction for the model output data

In all climate models, simulated climate for the baseline period differs more or less from its observational counterpart. For example, temperature biases are typically around a few degrees (e.g., Fig. 1 of Ruosteenoja et al., 2016). Consequently, if the GCM data by itself were used to calculate diverse climate indices (e.g., the number of warm summer days), the values obtained for the indices would be severely biased, for both the baseline-period and future climates.

To overcome this problem, an approach termed **bias correction** has been developed. This procedure consists of using model-produced daily-mean temperatures etc. both for the baseline period and for the future, but, using observational data, the simulated time series of the model output are adjusted to eliminate the systematic modelling errors. Precipitation and other climate quantities can be corrected by applying a similar philosophy. As discussed in Räisänen and Räty (2013), several alternative methods have been developed for bias correction.

In this project, we have produced bias-corrected data for daily mean, minimum and maximum temperatures, precipitation and wind speed. The method used for bias correction is called **quantile mapping**. The general idea of the method is outlined here, while a more detailed description is presented in Räisänen and Räty (2013). In applying the method, the GCM-simulated daily values of the different climate variables were first re-gridded onto the 10 x 10 km grid covering the area of Latvia using a bilinear interpolation. Thereafter, monthly correction functions were constructed for each grid-point and for each climate model by inspecting the differences between the quantiles of the frequency distribution of the respective variable as derived from observations (see section 2.6) and from the model output. The quantiles have been calculated for

the calibration period of 1966–2010. Formally, the observed (F_o) and modelled (F_c) cumulative probability distributions were used to transform the modelled time series (s_i) to the corrected time series (p_i):

$$p_i = F_o^{-1}(F_c(s_i)) \quad (1)$$

In calculating the correction functions, data were extracted, in addition to the target month, from the 15 nearest days of the previous and the subsequent calendar months. Such a two-month window, suggested by Räisänen and Räty (2013), was used to reduce sampling uncertainty in calculating the correction functions. A high number of quantiles, 1000 for each variable, were determined.

In carrying out the bias correction for precipitation, days with the observed precipitation smaller than $pr_{LIM,OBS} = 0.1$ mm/day were classified as dry. In order the modelled number of dry days during the calibration period to be equal to the observed number, we defined a corresponding model-based threshold value $pr_{LIM,MOD}$ for dry days for each location, month and climate model. Daily modelled precipitation rates below $pr_{LIM,MOD}$ were set to zero, and the corrected daily precipitation totals were calculated for wet days (i.e., those with $pr > pr_{LIM,MOD}$) only.

As an illustrative example, Fig. 7 shows the original and bias-corrected time series of model-simulated daily mean temperature for one summer season. In both time series, the temporal day-to-day course of temperature is in phase. However, in this particular GCM, in July and August modelled mean temperatures are somewhat lower than those observed, while in June there is a minor overestimation. In addition, the temporal variability of simulated temperatures tends to be slightly underestimated, in June in particular. In the corrected time series, these systematic biases have been eliminated.

Bias-corrected data were produced for seven quality-controlled global climate models (Table 2). We endeavoured to select a representative sub-ensemble of GCMs, so that there are models simulating both relatively weak and rather strong changes in mean temperature and precipitation (see Fig. 19 and Tables 9–11). Unfortunately, for wind speed, model output data were only

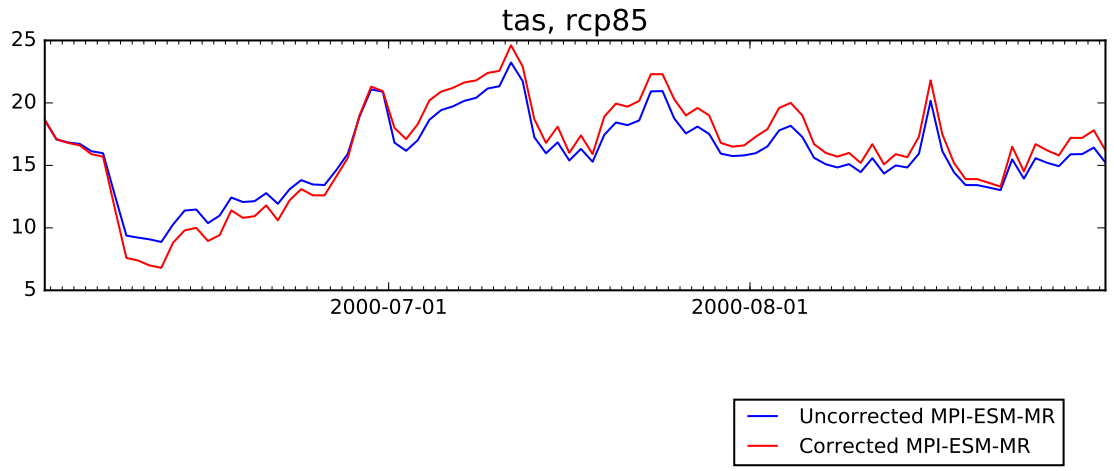

Figure 7. Time series of daily mean temperature simulated by MPI-ESM-MR for June-August of one model year at 57.1°N, 24.6°E. Original model output is denoted by a blue and corrected time series by a red line.

Table 2. Climate models for which the bias-corrected data were created. The first column depicts the model acronym and the other columns list the availability of the bias-corrected data for the diverse climate variables (T: surface air temperature; PR: precipitation; TXN: daily maximum and minimum temperatures; W: surface air wind speed).

Model	T	PR	TXN	W
MIROC5	X	X	X	-
HadGEM2-ES	X	X	X	X
MPI-ESM-MR	X	X	X	X
CNRM-CM5	X	X	X	-
GFDL-CM3	X	X	X	X
NCAR-CCSM4	X	X	X	-
CanESM2	X	X	X	-

available from three of these GCMs[2]. On the other hand, all seven GCMs provide simulations for all three greenhouse gas scenarios (RCP2.6, RCP4.5 and RCP8.5). The bias-corrected time series cover the period 1961–2100.

The main advantage of the present bias-correction algorithm is that the shape of the frequency distribution for the climate variables becomes realistic. For example, in the observation-based frequency distribution of temperature, values close to 0°C are far more common than values somewhat below or above zero (Fig. 8). This feature is distinctly more realistic in the bias-corrected than in the original model output data and is likewise evident in the distributions of the temperature variables representing future climate (in particular, in the daily minima). A reasonable representation of near-zero temperatures is essential for a reliable estimation of the count of freezing days, for instance.

For wind speeds, the MPI-ESM-MR model simulates only infinitesimally small changes (see Table 11 in the Appendix). Accordingly, even the bias-corrected future frequency distributions of wind speeds are nearly identical to those derived from the observations (Fig. 8).

Even so, the quantile mapping method involves drawbacks as well. Model-simulated temporally averaged changes in the different variables are not exactly preserved in the bias-corrected data. For example, warming may be, to some extent, more or less intense when derived from the bias-corrected data, compared with the original uncorrected model output. The problems are most severe in the coastal areas, where method-based uncertainties induced by both the Kriging interpolation of the observations and the bias correction of the climate data occur; e.g., the resulting relative errors in the projected mean warming may be up to about 20 %.

Concerning the utilization of the precipitation data, a further caveat has to be mentioned. In the bias-corrected data, daily precipitation values correlate in time far more strongly at adjacent grid points than in reality. Applications sensitive to the spatial correlation structures of precipitation, such as hydrological run-off and flood modelling, may thus suffer from a severe occasional over-estimation of area-integrated precipitation totals when these totals are calculated as a sum over

[2]In the procurement, bias-corrected data were promised for five climate GCMs at minimum. As bias corrections for wind speed could be given for three models only, we compensate this deficit by providing corrected data for the other variables from seven GCMs. Moreover, we provide projections for two climate indices (section 2.8) rather than a single one as it was stated in the procurement.

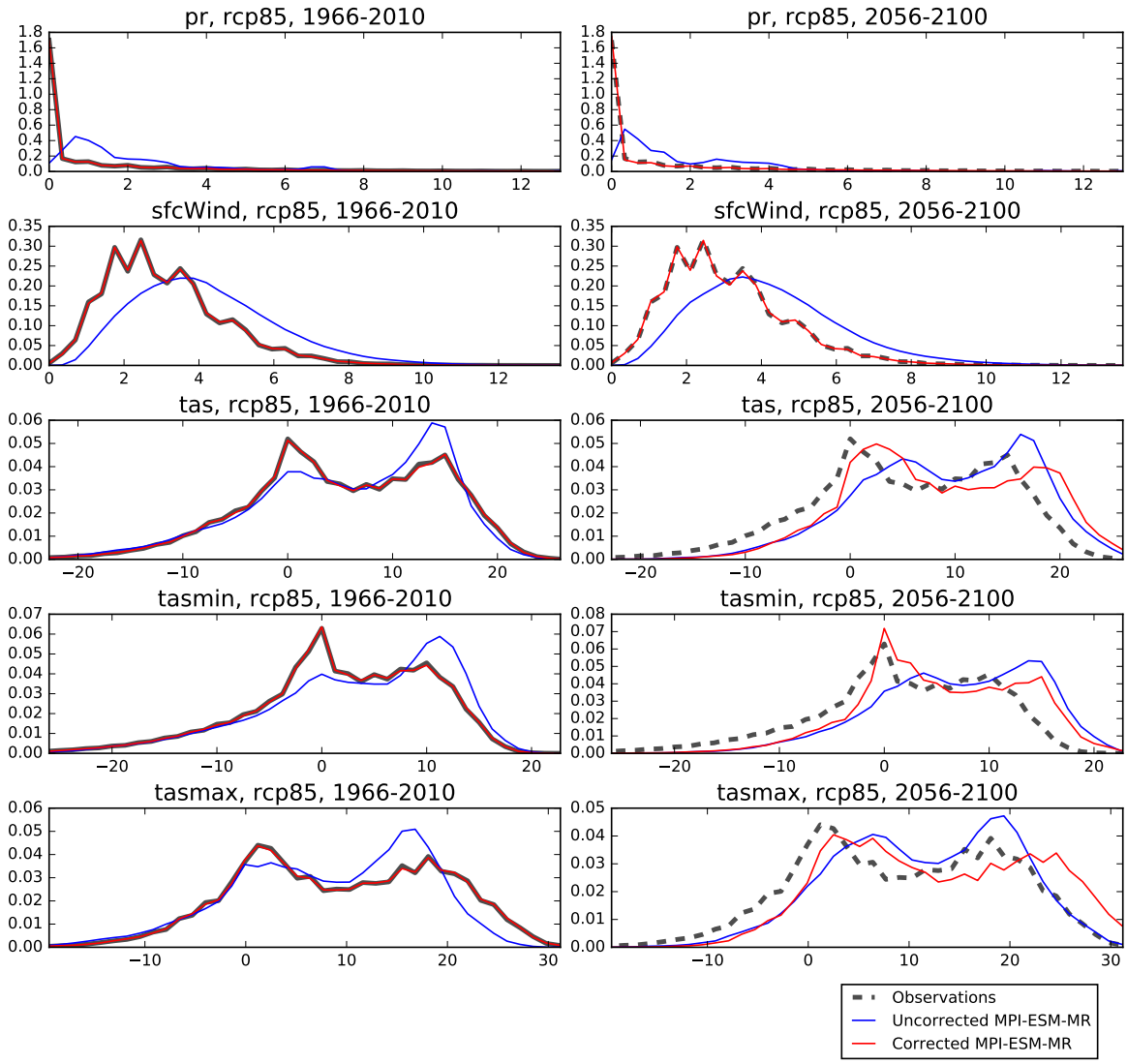

Figure 8. Frequency distributions of precipitation (panels on row 1), wind speed (row 2) and daily mean (row 3), minimum (row 4) and maximum temperature (row 5) as simulated by MPI-ESM-MR during the calibration period 1966–2010 (left panels) and the future period 2056–2100 under RCP8.5 (right panels); data from all Latvian grid points and all dates of the calibration period have been pooled. Frequency distributions derived directly from the original model output are denoted by a blue line, those from bias-corrected data by red. Observation-based distributions (representing the calibration period in both panels) are marked by a dashed black line. In the left-column panels, observational and bias-corrected distributions are virtually identical.

several adjacent grid cells. However, the statistics determined for the individual grid cells are not affected by this problem. Accordingly, we regard the present data sets as applicable to a majority of local impact models, such as crop and forest growth models.

The bias-corrected data have been stored in a space-saving NetCDF binary file format. This format is compatible with the most common data processing tools, such as the CDO, Python and R softwares.

2.8 Climate indices

Climate indices can be calculated from the bias-corrected model output files discussed in the previous subsection. Two temperature-based indices were calculated by FMI: the summer and ice day indices. To confirm the validity of the result, we first compiled our own Fortran code and then repeated the calculation using the CDO software developed at the Max-Planck-Institut für Meteorologie in Germany.

The bias-corrected data (section 2.7) have been sent to LEGMC to be used for calculation of the other relevant climate indices.

3 Spatial mean projections

3.1 Time series of changes

Future annual-mean trends in daily mean temperature and precipitation are shown in Fig. 9. Changes are 30-year running means presented relative to the baseline period (1971–2000) av-

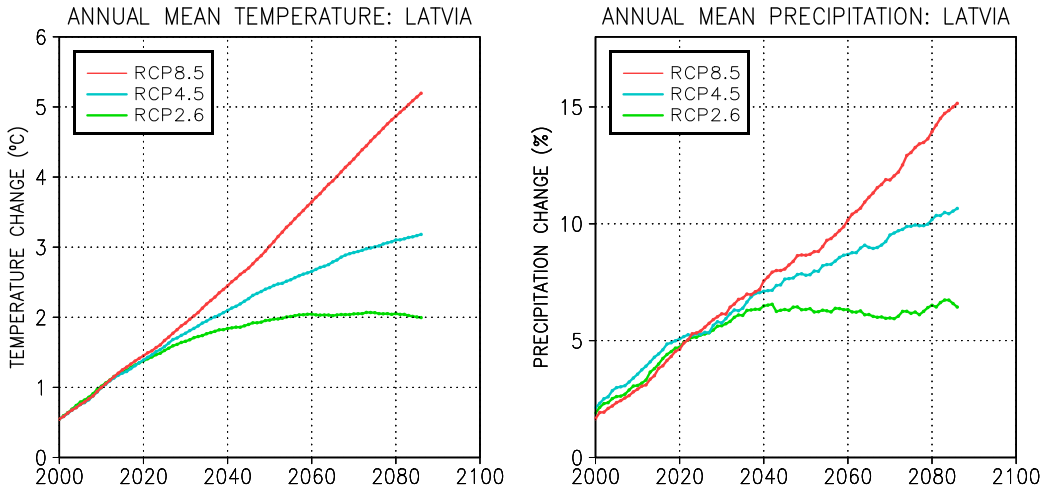

Figure 9. Projected multi-model mean changes in annual mean surface air temperature (in °C; left panel) and precipitation (in %; right panel) for the years 2000–2086, relative to the mean of the baseline period 1971–2000. All values are 30-year running means averaged spatially over Latvia. Projections are depicted separately for three greenhouse gas scenarios: RCP8.5, RCP4.5 and RCP2.6 (see the legend).

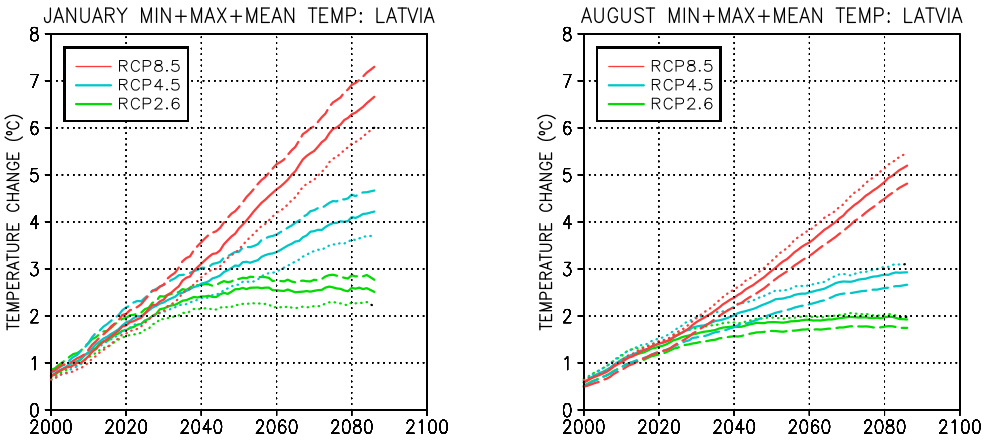

Figure 10. Projected multi-model mean changes in daily mean (solid curve), minimum (dashed curve) and maximum temperature (dotted curve) for the years 2000–2086, relative to the mean of the baseline period 1971–2000. Left panel represent January and right panel August; unit °C. All values are 30-year running means averaged spatially over Latvia. Projections are depicted separately for three greenhouse gas scenarios: RCP8.5, RCP4.5 and RCP2.6 (see the legend).

erage and are given separately for the RCP2.6, RCP4.5 and RCP8.5 scenarios. Only the multi-model mean changes are examined here.

During the first few decades of this century, annual mean temperature and precipitation increase at a similar rate according to all three RCP scenarios, but in the mid and, in particular, late 21st century projected changes depend substantially on the evolution of the greenhouse gas emissions. If the most detrimental RCP8.5 scenario is realized, annual mean temperature in Latvia is assessed to increase by about 5°C and precipitation by ∼15 %. According to the two mitigation scenarios (RCP2.6 and RCP4.5), projected changes are far weaker. The annual total of solar radiation (not shown) will increase by a few per cent, but this small increase is a residual of a drastic relative reduction in winter and a modest increase in summer and early autumn (Fig.14).

As a first approximation, daily minimum and maximum temperatures increase at a rate that is close to that projected for the daily means (Fig. 10). Nonetheless, there is a tendency towards increasing diurnal temperature amplitudes in summer, i.e., the daily maxima increase somewhat more rapidly than the daily minima. In winter, diurnal temperature variations diminish. This topic will be discussed in more detail in the next subsection.

3.2 Projections at a monthly level, including the uncertainty estimates

Monthly multi-model mean changes for the period 2071–2100, along with uncertainty intervals representing differences among the various GCM simulations, are presented for the various climate variables in Figs. 11, 12, 13, 14, 15, 16, 17 and 18. Note that figures have been given also for two variables not mentioned in the procurement (air pressure and solar radiation). The corresponding seasonal and annual mean projections for three future periods (2011–2040, 2041–2070 and 2071–2100), considering all three RCP scenarios, are given in Tables 3–8 in the Appendix.

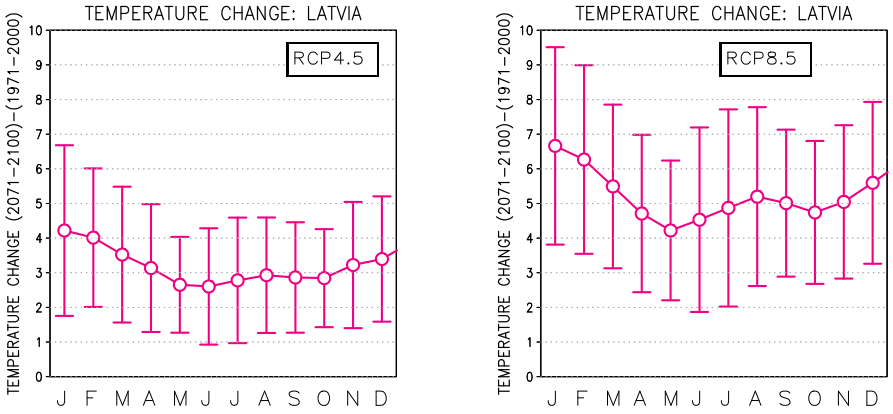

Figure 11. Projected changes in monthly mean temperature (°C) for the period 2071–2100, relative to 1971–2000; a spatial average over Latvia under RCP4.5 (left) and RCP8.5 (right). The curve denotes the best estimate for the change, i.e., the 28-model mean of the simulated temperature change. 90 % uncertainty intervals for the change, derived from the scatter among the individual GCM simulations, are marked by vertical bars. The x axis shows the months (J=January, F=February, etc.).

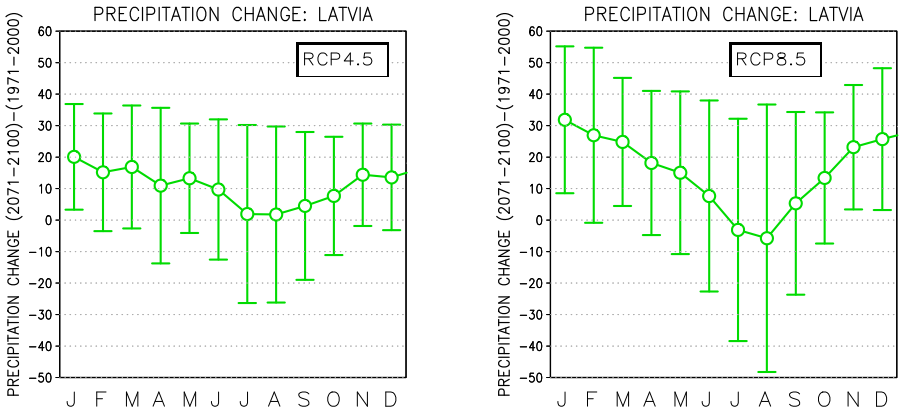

Figure 12. Projected changes in precipitation (in %) in Latvia from 1971–2000 to 2071–2100. For further information, see the caption of Fig. 11.

According to the multi-model mean, the temperature increase is strongest in mid-winter (according to RCP8.5, nearly 7°C per century), and there is a minor secondary maximum in warming in late summer (Fig. 11). Uncertainty intervals of the responses are fairly wide (e.g., from about 4°C to more than 9°C in January), but even the lower estimates (5th percentiles) for warming are positive throughout the year. For precipitation change, the multi-model mean projection is generally positive as well, with the exception of July and August under RCP8.5, but the error bars are very wide, so that the sign of change remains uncertain, apart from the cold season (Fig. 12).

Air pressure may decrease slightly, but considering the uncertainty estimates, this conclusion is far from certain (Fig. 13). Solar radiation is likely to decrease in winter (according to the multi-model mean under RCP8.5, by up to 10–15 % in December to February), while in late

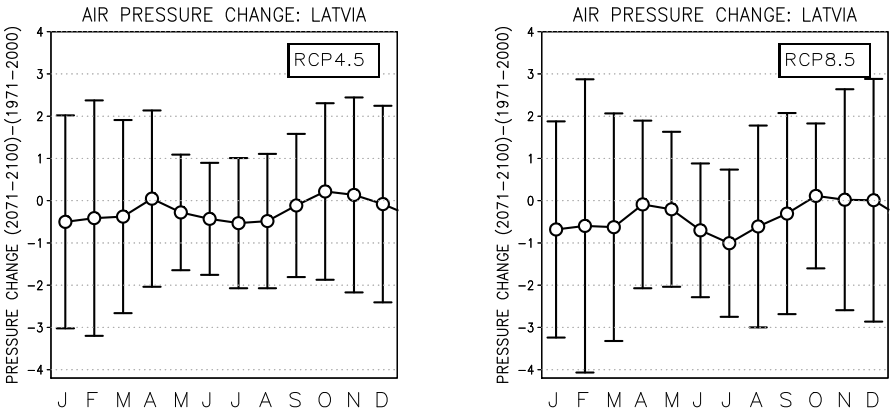

Figure 13. Projected changes in surface pressure (in hPa) in Latvia from 1971–2000 to 2071–2100. For further information, see the caption of Fig. 11.

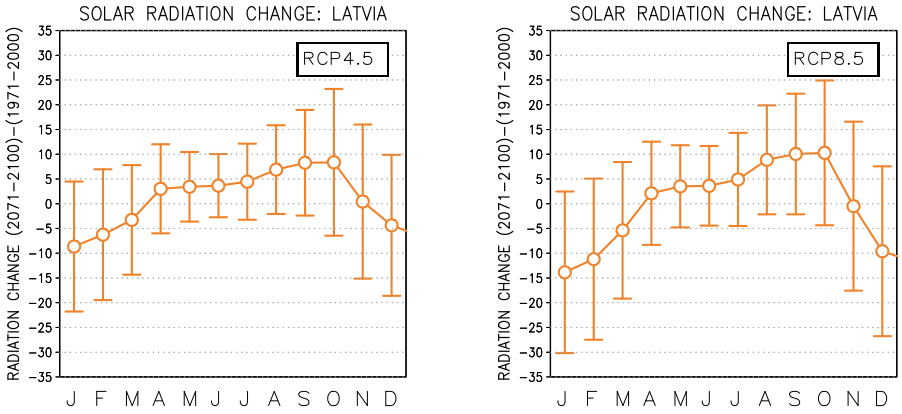

Figure 14. Projected changes in incident solar radiation at the surface (in %) in Latvia from 1971–2000 to 2071–2100. For further information, see the caption of Fig. 11.

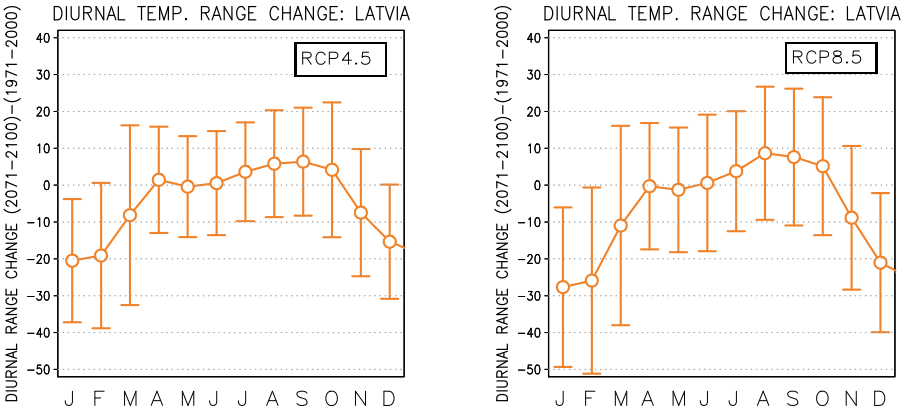

Figure 15. Projected changes in the diurnal temperature range (in %) in Latvia from 1971–2000 to 2071–2100. For further information, see the caption of Fig. 11.

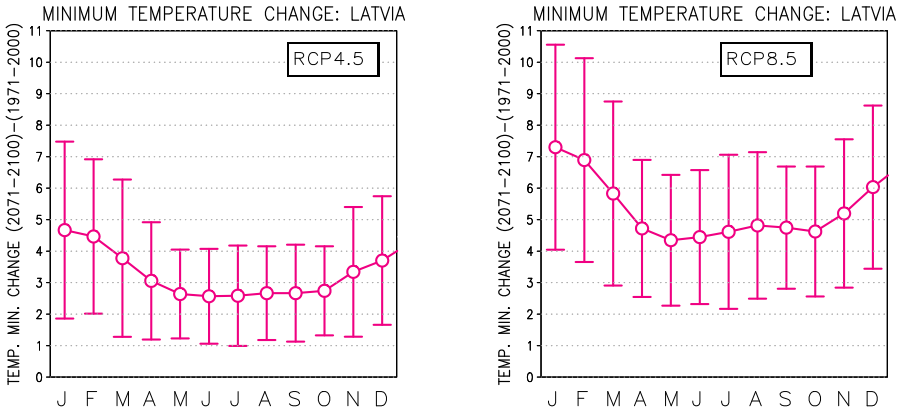

Figure 16. Projected changes in daily minimum temperatures (in °C) in Latvia from 1971–2000 to 2071–2100. For further information, see the caption of Fig. 11.

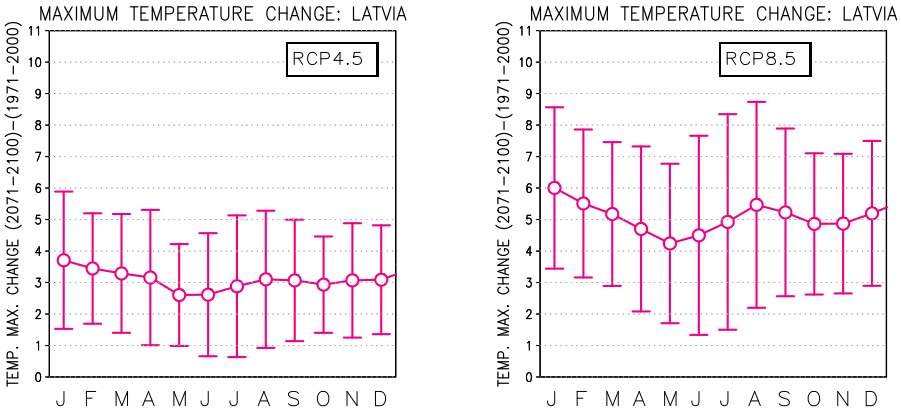

Figure 17. As in Fig. 16, but for the daily maximum temperatures.

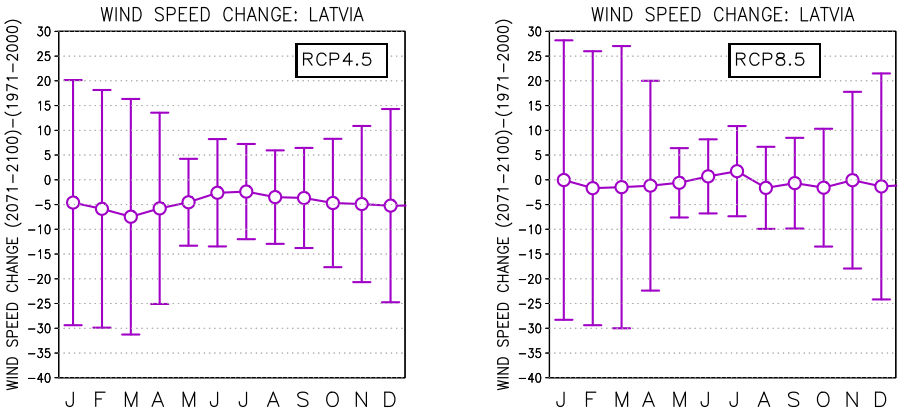

Figure 18. Projected changes in wind speeds (in %) in Latvia from 1971–2000 to 2071–2100. For further information, see the caption of Fig. 11.

summer and early autumn, the most probable projection is an increase of $\sim$10 % (Fig. 14). Even so, the 95 % uncertainty interval intersects the line of zero change in all months, and thus the sign of change is somewhat uncertain. Diurnal temperature range will decrease substantially in winter and possibly increase slightly in summer and early autumn (Fig. 15). Note that the seasonal course of the best-estimate change in daily maximum temperatures is clearly bimodal, with largest changes projected for January and August (Fig. 17). This kind of behaviour is far less evident for the daily minima (Fig. 16).

For wind speeds, the model projections are very contradictory (Fig. 18). The multi-model mean estimate for change is close to zero or slightly negative year-round, but considering the inter-model scatter, substantial increases or decreases of nearly $\pm$30 % are possible in winter under RCP8.5.

3.3 Dependencies among the projected changes in different climate variables

Spatially averaged changes in temperature, precipitation, solar radiation and diurnal temperature range in the individual GCMs are depicted in the form of scatter diagrams in Fig. 19. In the manifold of the model simulations, in winter the modelled temperature increase tends to correlate positively with the precipitation increase (a similar dependence was discovered by Räisänen and Ylhäisi (2015) in studying a large northern-European domain), while correlations with changes in solar radiation and diurnal temperature range are negative. These findings are physically plausible, since in winter in northern Europe, rainless weather, low temperatures and large diurnal temperature variations typically occur under clear weather conditions.

In summer, models producing largest warming tend to decrease precipitation and increase solar radiation and the amplitude of diurnal temperature range (Fig. 19, right panel). In contrast to winter, in warm season high temperatures are generally related to sunny and dry weather. This also explains the positive correlation between changes in the mean temperature and its diurnal range.

Fig. 19 has also been utilized in selecting a sub-ensemble of seven GCMs that simulate dissimilar changes in temperature and precipitation. These are the models for which bias-corrected data have been provided (Table 2).

3.4 Thermal growing season

Future evolution of the thermal growing season is explored at one grid point that resides close to Riga (Fig. 20). In the summer half of the year, projected warming is geographically very uniform across Latvia (Fig. 21). Accordingly, the projected changes for growing season parameters at that point are well representative for the entire country.

If the RCP8.5 scenario is realized, the onset of the growing season will become earlier by about one month, and the end of the season will be delayed somewhat more (Fig. 20). Growing degree days would increase from about 1500 to 2600. Under the RCP4.5 scenario, changes are qualitatively similar but less drastic.

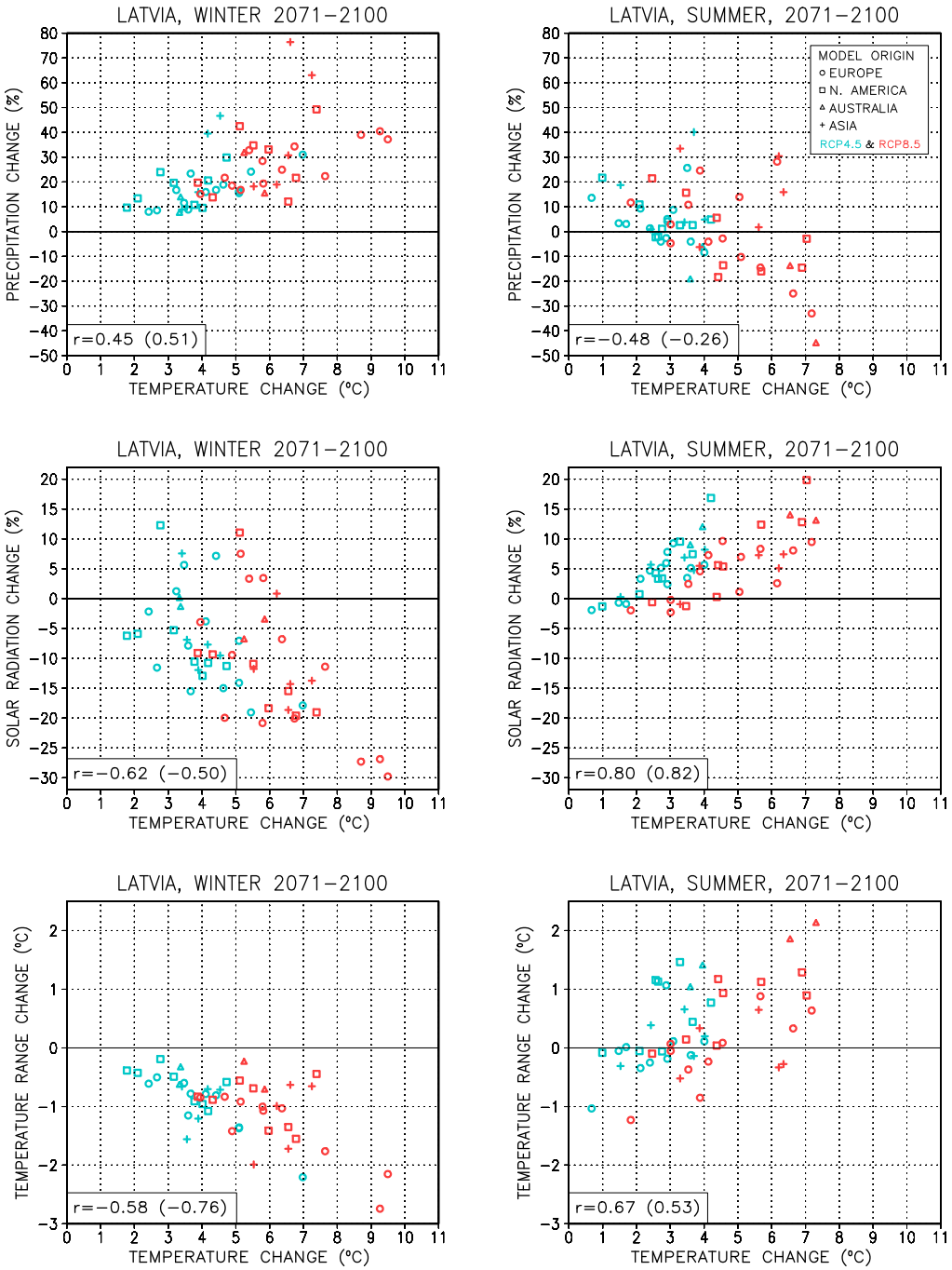

Figure 19. Scatter diagrams showing the simulated changes (from 1971–2000 to 2071–2100) in temperature, in conjunction with changes in precipitation (top), incident solar radiation (middle) and diurnal temperature range (bottom) in Latvia for the individual GCMs. Left panels depict the bivariate distributions for December-February, right panels for June-August; model simulations under RCP4.5 have been marked by blue and those under RCP8.5 by red symbols. To facilitate the identification of the responses produced by the individual GCMs in Tables 9–11, models originating from different continents have been marked by distinct symbols (see the legend). The correlation coefficients between the responses in the two variables under RCP8.5 (and for RCP4.5 in parentheses) are given in the bottom-left corner of each panel. Correlations higher than 0.37 are significant at the 5 % level, those over 0.48 at the 1 % level (when data available from 28 GCMs, implying $df = 26$).

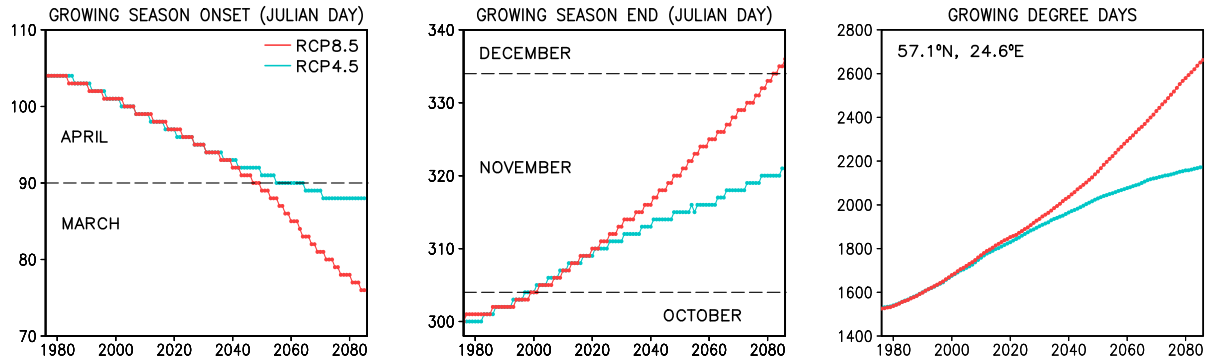

Figure 20. Temporal evolution of the onset (left) and termination (middle) of the thermal growing season (above 5°C) and the sum of growing degree days (right) at 57.125°N, 24.625°E. The dates of the onset and termination are given in Julian days; e.g., day 90 corresponds to 31 March and day 334 to 30 November.

4 Geographical distribution of the projected changes

Geographical distributions of projected changes in daily mean, minimum and maximum temperatures, precipitation and wind speeds are presented in Figs. 21–25. Compared with the large inter-model differences among the projected changes (Figs. 11–18), differences between the various regions of Latvia are generally fairly small.

In winter, warming tends to be somewhat stronger in the continental eastern provinces than in the areas of maritime climate in the west (Fig. 21). The difference is largest in January, when the multi-model mean warming ranges from about 5.4°C in the west to 7.2°C in the east (per 100 year, under RCP8.5). From April to October, projected temperature increase is very uniform across the country, with the intra-country differences being smaller than ∼0.5°C.

For the daily temperature minima and maxima, the geographical distribution of the change is qualitatively very similar to that of the mean temperature (Fig. 22–23). In winter, the intra-country differences are somewhat larger for the minima than for the maxima.

Precipitation tends to increase in the entire country throughout the year, apart from July and August (Fig. 24). In winter, the increase is slightly larger in the east than in the west. In summer and autumn, by contrast, precipitation projections tend to be dryest in the south. In all cases, however, geographical differences in the precipitation projection are smaller than 10 percentage points.

For wind speeds, the multi-model mean projections are very close to zero throughout the country over the entire year (Fig. 25). However, wind speed projections are extremely uncertain owing to a large inter-model scatter (Fig. 18).

5 Summer day and ice day indices

As an example, in this project two climate indices were calculated from the bias-corrected model output. The first one, summer day index SU25 (Fig. 26), gives the annual number of days

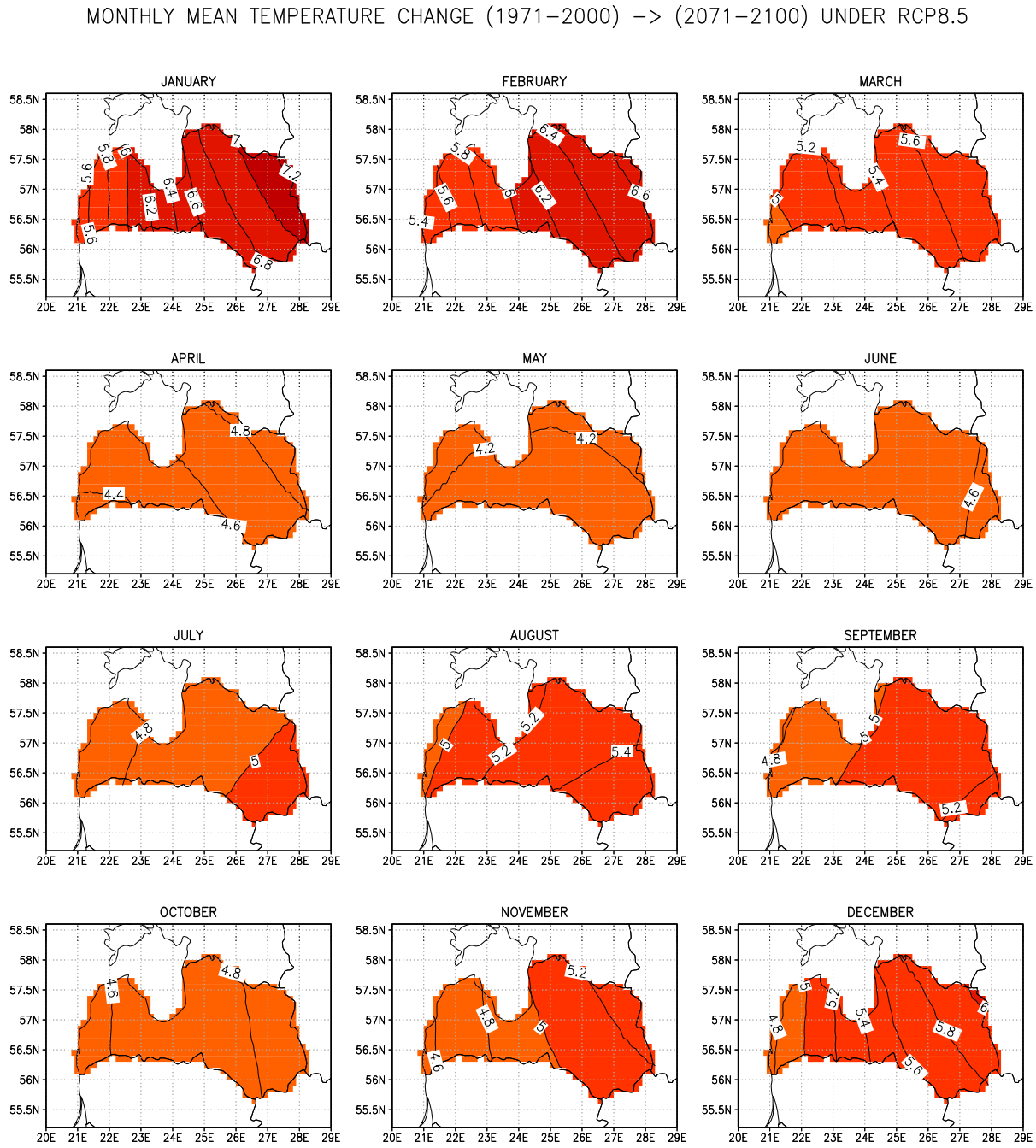

Figure 21. Geographical distribution of projected changes in monthly mean temperatures in Latvia from 1971–2000 to 2071–2100 under the RCP8.5 scenario; an average of the simulations performed with 28 GCMs. Unit °C.

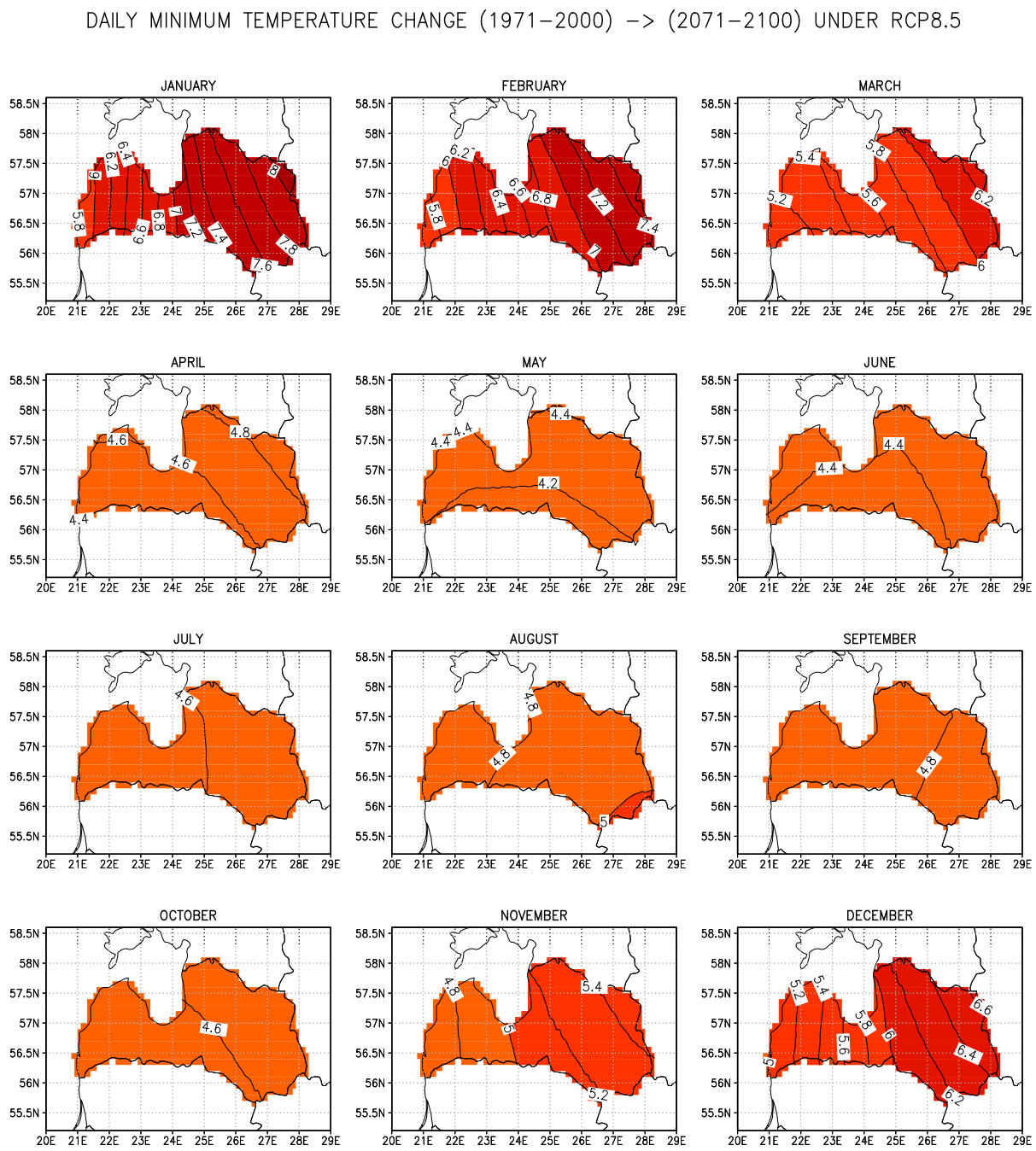

Figure 22. As in Fig. 21 but for the temporally-averaged daily minimum temperature (an average of 25 GCMs).

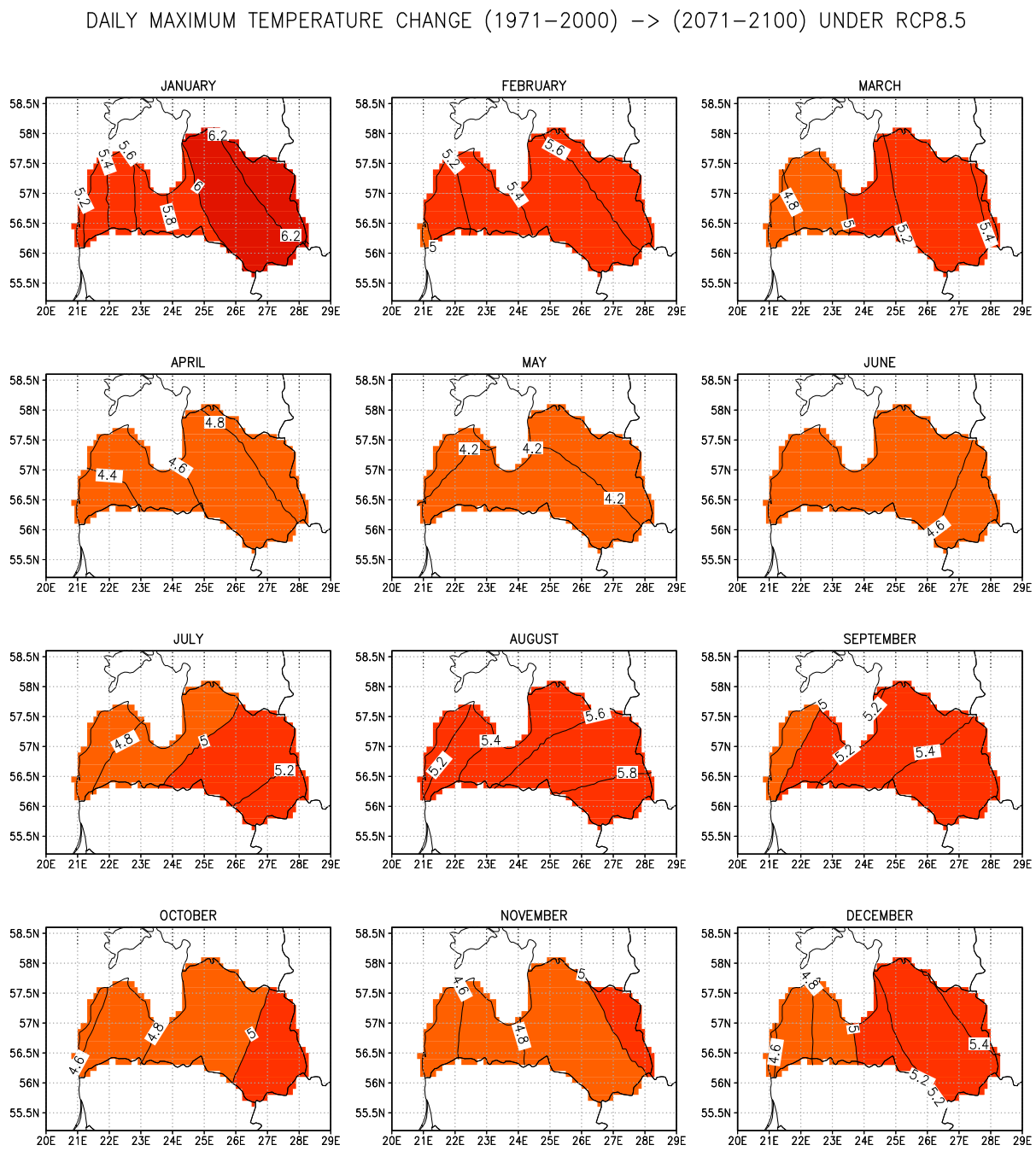

Figure 23. As in Fig. 21 but for the temporally-averaged daily maximum temperature (an average of 25 GCMs).

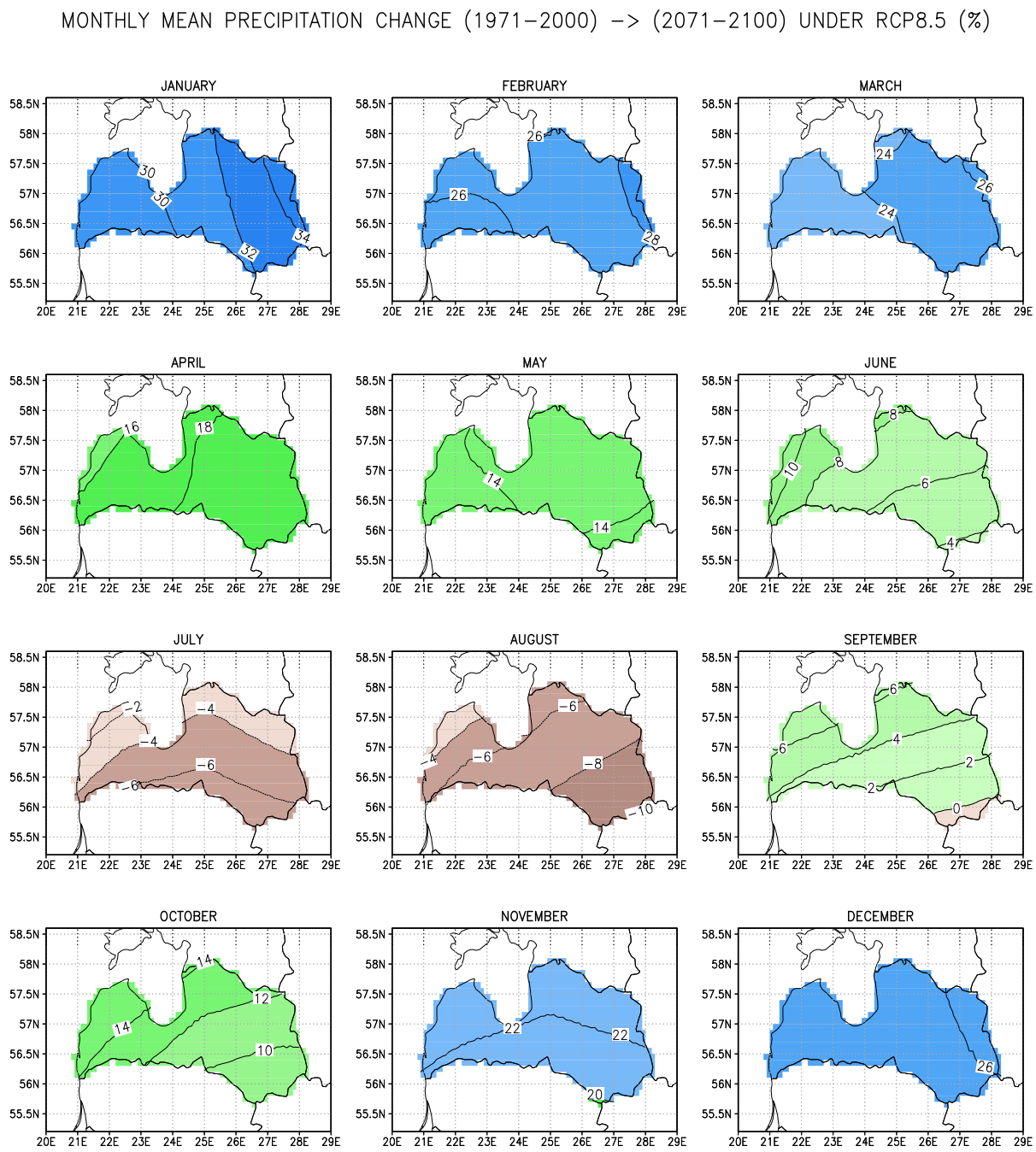

Figure 24. Projected changes in monthly precipitation totals (in %) from 1971–2000 to 2071–2100 under RCP8.5; an average of the simulations performed with 28 GCMs.

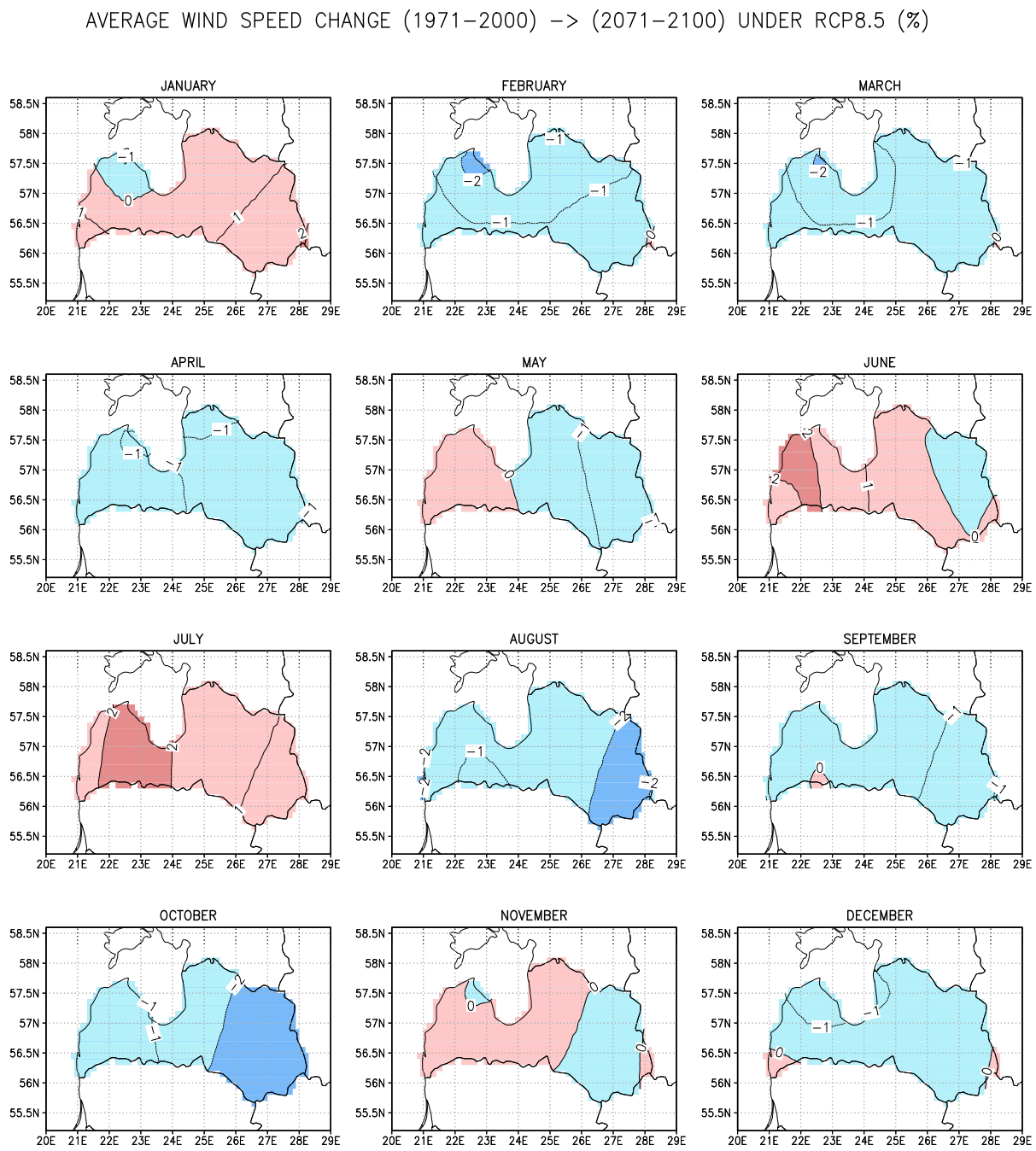

Figure 25. Projected change in average wind speeds (in %) from 1971–2000 to 2071–2100 under RCP8.5; an average of the simulations performed with 24 GCMs.

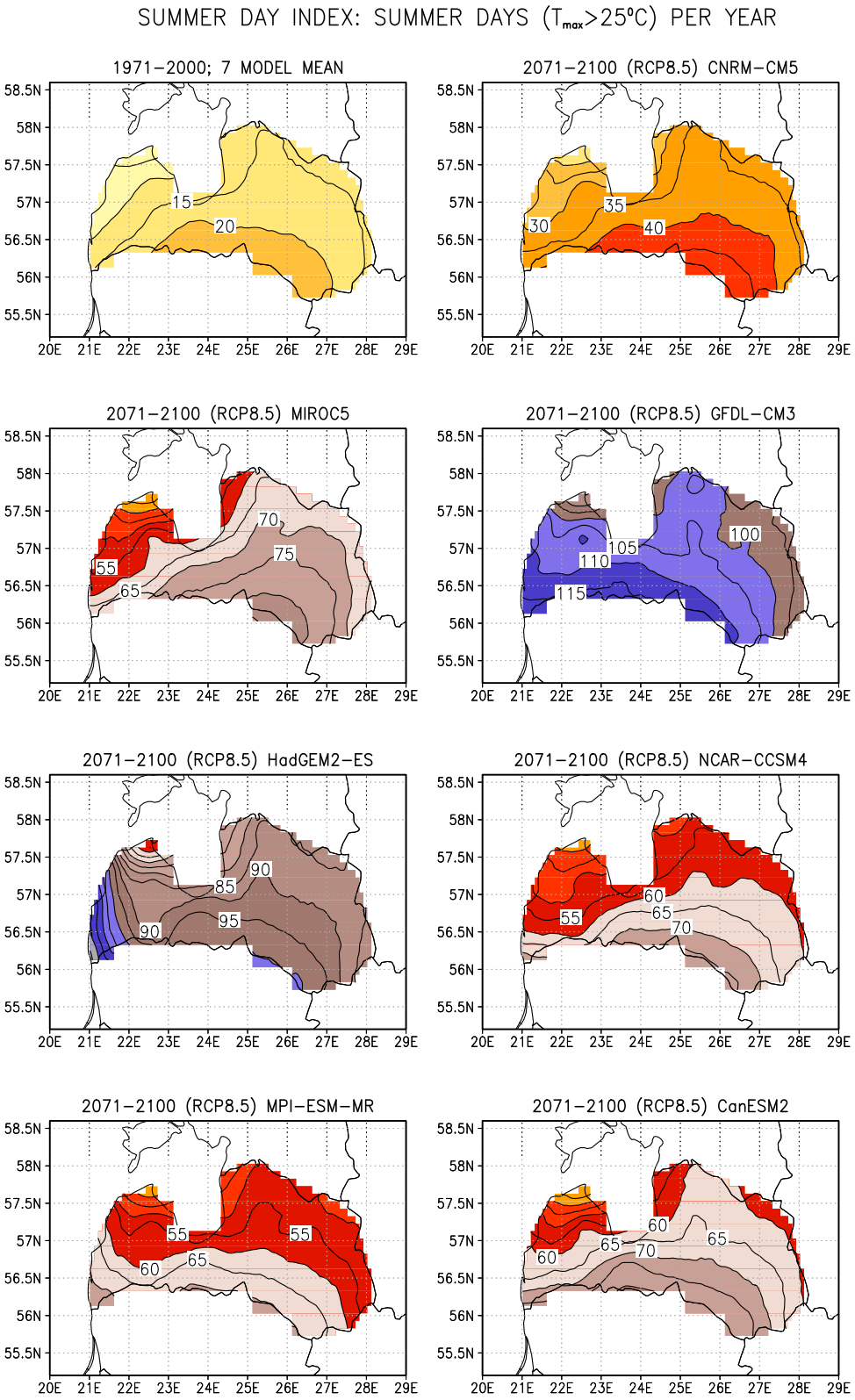

Figure 26. Model-simulated count of summer days with a maximum temperature above +25°C (the summer day index SU25). The top-left panel shows the average count during the period 1971–2000 (a mean of the values calculated from the bias-corrected simulations performed with the seven GCMs). The remaining panels depict estimates for the index for the period 2071–2100 under RCP8.5, derived separately for the individual GCMs; the model acronym is given above each panel.

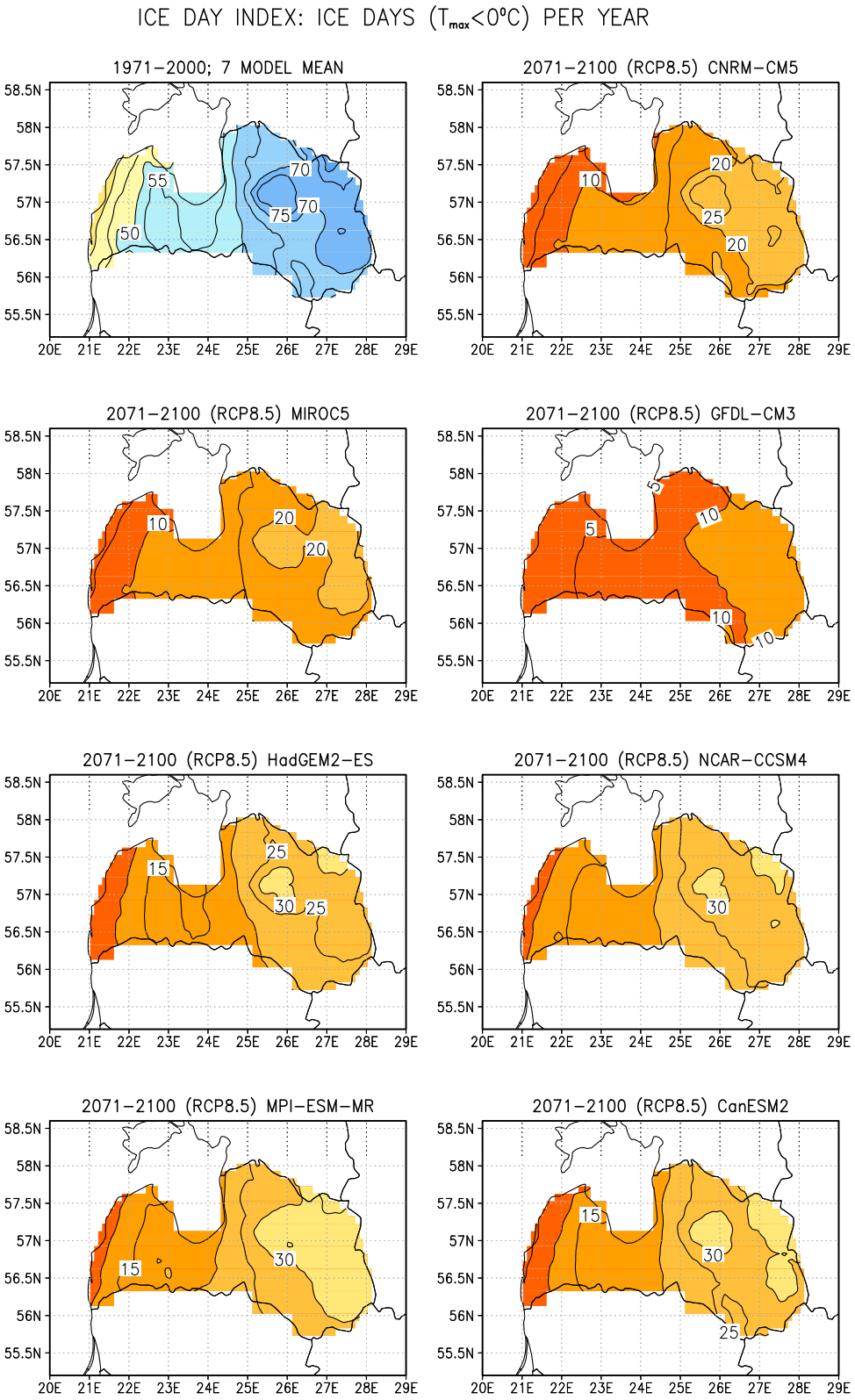

Figure 27. Model-simulated number of ice days with a maximum temperature below 0°C (the ice day index ID0). The top-left panel shows the average count during the period 1971–2000 and the remaining panels corresponding estimates for the period 2071–2100 under RCP8.5, separately for the individual GCMs (see the explanation of Fig. 26).

with a maximum temperature of higher than +25°C. Correspondingly, the second index, ice day index ID0 (Fig. 27), yields the number of days with a maximum temperature below zero. For both indices, only the average estimate of the seven GCM is presented for the baseline period 1971–2000, since for that period the estimates derived from the individual bias-corrected model simulations are virtually identical. For future climate (in this example, 2071–2100 under RCP8.5), by contrast, estimates are given separately for all seven GCMs.

In the baseline-period climate, the average number of summer days per year ranged from less than 5 in the northern Kurzeme region to more than 20 in the Zemgale region. As a response to anticipated warming, the number increases dramatically. Even so, there is a large divergence across the individual model projections. According to the most modest estimate (CNRM-CM5), the projected number in 2071–2100 under RCP8.5 would be about 20 in the north-west and nearly 50 in the south-east. Conversely, in the bias-corrected simulation of GFDL-CM3, the average future number of summer days would be close to 100 and even larger in the southern provinces.

The average number of ice days varied in 1971–2000 from less than 40 in the vicinity of the Baltic Sea coast to 70–80 in continental north-eastern Latvia. Moreover, the number tends to be larger in elevated areas than in the nearby lowlands. As a consequence of projected warming, the number of ice days declines, but again, the inter-model differences are substantial. On the basis of the GFDL-CM3 simulation, there would be only a few ice days per winter in the west and slightly more than 10 in the east. According to MPI-ESM-MR, the average number would remain higher than 30 in wide areas in the east and be less than 10 only in the vicinity of the western coast.

In comparing projected changes in the climate indices to modelled changes in long-term mean temperatures (Table 11), one must bear in mind that the bias correction algorithm distorts changes in the temperature variables to some extent; under RCP8.5 by late 21st century, the largest method-induced differences are $\sim \pm 1$°C. Moreover, in calculating the indices, only one parallel run has been considered, while the responses listed in Tables 9–11 are averages over all parallel runs available for each individual GCM (Table 1). Therefore, projected changes in the index values (Figs. 26–27) are not entirely consistent with the changes in temperature maxima shown in Table 11. The same feature concerns precipitation and wind speed -derived indices as well.

6 Climate extremes and the distribution of wind directions

In this project, future changes in the occurrence of extreme weather events and in the distribution of wind directions have been discussed only qualitatively. All the inferences are founded on experiments performed with the previous (CMIP3) model generation that was used in compiling the 4th assessment report of IPCC (2007).

According to Jylhä et al. (2015), day-to-day variations in temperature appear to diminish in northern Europe in winter, whereas no substantial changes in the variability are simulated for summer. Thus, one can deduce that the most extreme cold temperatures in winter will rise **more** than monthly mean temperatures of that season. In other words, in conjunction with the general warming tendency, winter temperature climate would become **less extreme** than recently.

Conversely, in summer, the highest temperatures are anticipated to increase approximately at a similar rate as the mean temperatures do.

In summer in northern Europe, precipitation climate is projected to become, to some degree, increasingly extreme (Lehtonen et al., 2014a). This indicates that heavy precipitation events would become even more extreme while dry periods between the events would lengthen. However, in precipitation, natural year-to-year variability is very strong, and therefore it is unlikely that any signal towards more extreme conditions would be discernible in the observations in the immediate future. In winter, the substantial increase in mean precipitation manifests itself both as an increase in the frequency of wet days and as an increase in precipitation totals falling in those days.

Future trends in extremely strong winds are likely to be qualitatively similar to those in long-term mean wind speeds (Gregow et al., 2012). According to the multi-model mean projection (Figs. 18 and 25), monthly mean wind speeds seem to remain nearly unchanged in the future. This might indicate that no radical changes would occur in extremely strong winds either. Nonetheless, due to the large uncertainty in the mean wind speed projections (Fig. 18), this conclusion is very tentative.

As a continuation of the present project, climatologists in LEGMC will use a limited sub-ensemble of bias-corrected GCM simulations (section 2.7) to assess future changes in a number of climate indices, including indices representing diverse climate extremes. These analyses will reveal whether the above-mentioned inferences hold true for those CMIP5 model simulations.

Räisänen and Ylhäisi (2015) showed that mean summer temperatures in northern Europe are projected to increase slightly more rapidly according to the CMIP5 than CMIP3 GCMs. In other seasons, there is no statistically significant difference in the magnitude of warming. Annual precipitation totals appear to increase somewhat less according to the recent model generation, but owing to a large inter-model scatter, no significant differences are evident in the precipitation responses of any individual calendar season.

In principle, this kind of differences between the successive model generations should be reflected in the projected changes in the various temperature and precipitation-based climate indices. However, as stated by Räisänen and Ylhäisi (2015), "...the differences in temperature and precipitation change between the ensembles remain relatively small compared with the variation between the individual model simulations". Therefore, it is not possible to know in advance whether changes in the indices derived from the present 7-GCM ensemble will be less or more intense than those inferred previously from the CMIP3 GCMs. Qualitatively, it is likely that the direction of the changes will generally be the same.

Regarding the wind directions, westerly and south-westerly winds seem to become increasingly frequent in northern Europe in autumn and winter, at the expense of winds blowing from the east (Ruosteenoja et al., 2013). This is in concordance with the surface air pressure projections, according to which long-term mean air pressure is falling over the Arctic Sea and rising in Central Europe (Ruosteenoja et al., 2013; Räisänen and Ylhäisi, 2015). In spring and summer, projected changes in the wind speed distribution appeared to be less prominent.

7 Concluding remarks

Owing to the continuously proceeding global warming, the future climate in Latvia is likely to be fairly different from that having prevailed during recent decades. In winter in particular, conditions are anticipated to become much warmer and wetter than recently, and less solar radiation will be received. Concurrently, diurnal temperature range is projected to decrease. The tendency towards warmer and wetter conditions appears to be strongest in the eastern parts of the country. The number of ice days will decline substantially everywhere.

In summer, warming is projected to be somewhat weaker than in winter and precipitation might even reduce slightly. Summer days with a maximum temperature above 25°C will become much more frequent than recently, and the length and degree days of the thermal growing season will increase. On the other hand, average wind speeds may remain nearly unchanged throughout the year.

According to the previous climate model generation, temporal variations in winter temperatures would dampen in the future, and extremely low temperatures would thus rise drastically. In summer, there would be no notable change in the variability and thus low and high temperatures seem to increase at a similar rate. Summertime precipitation climate, by contrast, may become more fluctuating.

In the framework of the present project, we have produced bias-corrected data for a number of GCMs. Bias correction consists of finding correction factors that eliminate the major differences between the model-simulated and observed climate during recent decades. The same correction factors are then applied for adjusting the simulations of future climate. Observational analyses needed for the correction procedure have been created by using Kriging interpolation. Although widely used in climate research, that interpolation method typically involves problems close to the boundaries of the inspected area. For daily mean, minimum and maximum temperatures, for instance, the outcome of the Kriging analyses seem to be less reliable near the eastern boundary of Latvia. As the bias-corrected model output is applied to calculating diverse climate indices, the resulting index values for regions close to the boundaries should therefore be considered with caution.

Increasing summer temperatures projected for Latvia, in conjunction with nearly unchanged or even decreasing precipitation, tend to reduce soil moisture content in the future. This may deteriorate the conditions of agriculture and forestry, increase forest fire ignition (Lehtonen et al., 2014b) and induce occasional low water levels and exceptionally small discharge in rivers. On the other hand, agriculture production may benefit from long and warm growing seasons (e.g., Ruosteenoja et al., 2016, and references therein), and the need for heating energy in buildings decreases (Jylhä et al., 2015). Various implications of climate change will be discussed in more detail in the other sub-task of the present project.

Projected climatic changes are subject to a substantial inter-model scatter. In addition, the magnitude of change depends on the evolution of the greenhouse gas emissions; this challenge has been addressed here by elaborating projections separately for three greenhouse gas scenarios of varying severity. Accordingly, all decisions concerning adaptation to the future climate must be based on rather uncertain quantitative information. In any case, the general tendency towards a warmer and, in winter, wetter climate in the future is evident.

8 List of deliverables

During the project, the following files and reports have been provided:

1. A report about the commencement of the project (in April of 2016).
2. Projected monthly-mean changes in daily mean, minimum and maximum temperature, precipitation and wind speed on a 10 x 10 km grid covering Latvia: csv files containing overlapping 30-year running means for 112 periods from 1960–1979 to 2071–2100, separately for three RCP scenarios (in May, see section 2.4).
3. Bias-corrected daily mean, minimum and maximum temperature and precipitation on a 10 x 10 km grid covering Latvia (NetCDF files) from seven climate models; for wind speed, from three models (section 2.7). The models were chosen by inspecting the joint distribution of projected changes in temperature and precipitation in Latvia, so that this sub-ensemble of models representatively contains both models projecting relatively small and large changes in these variables (in June).
4. Two selected temperature-based climate indices calculated from these bias-corrected model output files (in June; see section 2.8).
5. Spatially averaged changes in daily mean, minimum and maximum temperature, precipitation and wind speed, including both multi-model means and uncertainty estimates (in September, section 3).

Observation-based analyses of mean, minimum and maximum temperature and precipitation have been created at LEGMC in March-April of 2016 by the third author of this report (section 2.6).

Acknowledgments

The CMIP5 GCM data were downloaded from the EARTH System Grid Federation data archive (http://pcmdi9.llnl.gov). Tiina Ervasti is acknowledged for useful comments.

References

Aalto, J., P. Pirinen, and K. Jylhä, 2016: New gridded daily climatology of Finland — Permutation-based uncertainty estimates and temporal trends in climate. *Journal of Geophysical Research — Atmospheres*, doi:10.1002/2015JD024651.

Gregow, H., K. Ruosteenoja, N. Pimenoff, and K. Jylhä, 2012: Changes in the mean and extreme geostrophic wind speeds in Northern Europe until 2100 based on nine global climate models. *International Journal of Climatology*, **32**, 1834–1846, doi:10.1002/joc.2398.

Haylock, M. R., N. Hofstra, A. M. G. Klein Tank, E. J. Klok, P. D. Jones, and M. New, 2008: A European daily high-resolution gridded dataset of surface temperature and precipitation for 1950–2006. *J. Geophys. Res.*, **113 (D20)**, doi:10.1029/2008JD010201.

IPCC, 2007: *Climate Change 2007: The physical science basis. Contribution of Working Group I to the Fourth Assessment Report of the Intergovernmental Panel on Climate Change.* Cambridge University Press, Cambridge, U.K., 996 pp, [S. Solomon, D. Qin, M. Manning, Z. Chen, M. Marquis, K. B. Averyt, M. Tignor and H. L. Miller (eds.)].

IPCC, 2013: *Climate Change 2013: The physical science basis. Contribution of Working Group I to the Fifth Assessment Report of the Intergovernmental Panel on Climate Change.* Cambridge University Press, Cambridge, U.K., 1535 pp, [Stocker, T.F., D. Qin, G.-K. Plattner, M. Tignor, S.K. Allen, J. Boschung, A. Nauels, Y. Xia, V. Bex and P.M. Midgley (eds.)].

Jaagus, J. and K. Mändla, 2014: Climate change scenarios for Estonia based on climate models from the IPCC Fourth Assessment Report. *Estonian Journal of Earth Sciences*, **63**, 166–180, doi: 10.3176/earth.2014.15.

Jylhä, K., K. Ruosteenoja, J. Räisänen, A. Venäläinen, H. Tuomenvirta, L. Ruokolainen, S. Saku, and T. Seitola, 2009: Arvioita Suomen muuttuvasta ilmastosta sopeutumistutkimuksia varten — ACCLIM-hankkeen raportti 2009 (The changing climate in Finland: estimates for adaptation studies. ACCLIM project report 2009.). Raportteja 2009:4, Ilmatieteen laitos, 102 pp. (In Finnish, extended abstract also in English).

Jylhä, K., et al., 2015: Energy demand for the heating and cooling of residental houses in Finland in a changing climate. *Energy and Buildings*, **99**, 104–116, doi:10.1016/j.enbuild.2015.04.001.

Lehtonen, I., K. Ruosteenoja, and K. Jylhä, 2014a: Projected changes in European extreme precipitation indices on the basis of global and regional climate model ensembles. *Int. J. Climatol.*, **34**, 1208–1222, doi:10.1002/joc.3758.

Lehtonen, I., K. Ruosteenoja, A. Venäläinen, and H. Gregow, 2014b: The projected 21st century forest-fire risk in Finland under different greenhouse gas scenarios. *Boreal Environment Research*, **19**, 127–139.

Lind, P. and E. Kjellström, 2008: Temperature and precipitation changes in Sweden; a wide range of model-based projections for the 21st century. Reports Meteorology and Climatology 113, Swedish Meteorological and Hydrological Institute, S-60176 Norrköping, Sweden. www.smhi.se/polopoly_fs/1.3297!RMK113_rapport_090421.pdf.

Luomaranta, A., K. Ruosteenoja, K. Jylhä, H. Gregow, J. Haapala, and A. Laaksonen, 2014: Multimodel estimates of the changes in the Baltic Sea ice cover during the present century. *Tellus A*, **66**, 22 617, doi:http://dx.doi.org/10.3402/tellusa.v66.22617.

Meleshko, V. P., V. M. Kattsov, V. A. Govorkova, P. V. Sporyshev, I. M. Shkol'nik, and B. E. Shneerov, 2008: Climate of Russia in the 21st century. Part 3. Future climate changes calculated with an ensemble of coupled atmosphere-ocean general circulation CMIP3 models. *Russian Meteorology and Hydrology*, **33**, 541–552, doi:10.3103/S106837390809001X.

Räisänen, J. and O. Räty, 2013: Projections of daily mean temperature variability in the future: cross-validation tests with ENSEMBLES regional climate simulations. *Clim Dyn*, **41**, 1553–1568, doi: 10.1007/s00382-012-1515-9.

Räisänen, J. and J. S. Ylhäisi, 2015: CO_2-induced climate change in northern Europe: CMIP2 versus CMIP3 versus CMIP5. *Climate Dynamics*, **45**, 1877–1897, doi:10.1007/s00382-014-2440-x.

Ruosteenoja, K., J. Räisänen, K. Jylhä, H. Mäkelä, I. Lehtonen, H. Simola, A. Luomaranta, and S. Weiher, 2013: Maailmanlaajuisiin CMIP3-malleihin perustuvia arvioita Suomen tulevasta ilmastossa (Climate change estimates for Finland on the basis of global CMIP3 climate models). Raportteja 2013:4, Ilmatieteen laitos, 83 pp. (In Finnish with abstract in English and Swedish).

Ruosteenoja, K., J. Räisänen, A. Venäläinen, and M. Kämäräinen, 2016: Projections for the duration and degree days of the thermal growing season in Europe derived from CMIP5 model output. *International Journal of Climatology*, **36**, 3039–3055, doi:10.1002/joc.4535.

Ruosteenoja, K., H. Tuomenvirta, and K. Jylhä, 2007: GCM-based regional temperature and precipitation change estimates for Europe under four SRES scenarios applying a super-ensemble pattern-scaling method. *Climatic Change*, **81**, 193–208, doi:10.1007/s10584-006-9222-3.

van Vuuren, D. P., et al., 2011: The representative concentration pathways: an overview. *Climatic Change*, **109**, 5–31, doi:10.1007/s10584-011-0148-z.

Appendix: Tables of changes averaged spatially over Latvia

This Appendix provides estimates for future climatic changes in Latvia in tabular form. Multi-model mean changes in different variables, in conjunction with the 90 % uncertainty intervals and separately for three RCP scenarios, are given in Tables 3-8. Projections simulated by the individual climate models are presented in Tables 9–11.

Table 3. Projected seasonal and annual mean changes in surface air temperature (in °C) relative to 1971–2000; spatial averages over Latvia (DJF: December to February; MAM: March to May; JJA: June to August; SON: September to November; ANN: annual mean). Projections are given separately for three 30-year future periods and three RCP forcing scenarios. For each projection, three quantiles are given, with the median standing for the best estimate of the change and the 5. and 95. percentage points defining the 90 % probability interval. The quantiles are derived from a normal distribution fitted to the multi-model data.

Period	Forcing	Quantile	DJF	MAM	JJA	SON	ANN
2011–2040	RCP2.6	5 %	0.4	0.5	0.5	0.5	0.7
2011–2040	RCP2.6	Median	1.9	1.5	1.5	1.4	1.6
2011–2040	RCP2.6	95 %	3.3	2.6	2.4	2.3	2.4
2011–2040	RCP4.5	5 %	0.5	0.6	0.5	0.5	0.8
2011–2040	RCP4.5	Median	2.0	1.6	1.5	1.4	1.6
2011–2040	RCP4.5	95 %	3.5	2.7	2.5	2.4	2.5
2011–2040	RCP8.5	5 %	0.6	0.7	0.5	0.7	0.9
2011–2040	RCP8.5	Median	2.0	1.7	1.6	1.6	1.7
2011–2040	RCP8.5	95 %	3.5	2.7	2.7	2.4	2.6
2041–2070	RCP2.6	5 %	1.0	0.8	0.6	0.8	1.0
2041–2070	RCP2.6	Median	2.4	2.1	1.8	1.8	2.0
2041–2070	RCP2.6	95 %	3.7	3.3	3.1	2.9	3.1
2041–2070	RCP4.5	5 %	1.2	1.1	0.9	1.2	1.3
2041–2070	RCP4.5	Median	3.1	2.6	2.3	2.3	2.6
2041–2070	RCP4.5	95 %	5.0	4.0	3.7	3.4	3.8
2041–2070	RCP8.5	5 %	2.4	1.6	1.3	2.0	2.1
2041–2070	RCP8.5	Median	4.1	3.1	3.1	3.2	3.4
2041–2070	RCP8.5	95 %	5.9	4.7	4.9	4.5	4.8
2071–2100	RCP2.6	5 %	1.0	0.6	0.5	0.8	0.9
2071–2100	RCP2.6	Median	2.4	1.9	1.8	1.9	2.0
2071–2100	RCP2.6	95 %	3.7	3.3	3.1	2.9	3.1
2071–2100	RCP4.5	5 %	2.0	1.6	1.2	1.5	1.8
2071–2100	RCP4.5	Median	3.9	3.1	2.8	3.0	3.2
2071–2100	RCP4.5	95 %	5.7	4.6	4.4	4.4	4.5
2071–2100	RCP8.5	5 %	3.7	2.8	2.2	3.0	3.3
2071–2100	RCP8.5	Median	6.2	4.8	4.9	4.9	5.2
2071–2100	RCP8.5	95 %	8.6	6.8	7.5	6.9	7.1

Table 4. Projected seasonal and annual mean changes in precipitation (in %) for Latvia; for further information, see the caption of Table 3.

Period	Forcing	Quantile	DJF	MAM	JJA	SON	ANN
2011–2040	RCP2.6	5 %	-2	-4	-12	-5	-1
2011–2040	RCP2.6	Median	8	7	2	5	5
2011–2040	RCP2.6	95 %	17	18	15	15	11
2011–2040	RCP4.5	5 %	-4	-2	-16	-6	-2
2011–2040	RCP4.5	Median	7	8	2	4	5
2011–2040	RCP4.5	95 %	19	18	19	15	13
2011–2040	RCP8.5	5 %	-1	-3	-12	-6	0
2011–2040	RCP8.5	Median	8	9	1	4	6
2011–2040	RCP8.5	95 %	17	21	15	14	11
2041–2070	RCP2.6	5 %	-3	-1	-13	-5	-2
2041–2070	RCP2.6	Median	8	8	3	6	6
2041–2070	RCP2.6	95 %	19	18	18	16	15
2041–2070	RCP4.5	5 %	0	-1	-16	-6	0
2041–2070	RCP4.5	Median	13	11	1	8	8
2041–2070	RCP4.5	95 %	26	24	19	22	17
2041–2070	RCP8.5	5 %	1	4	-23	-6	-1
2041–2070	RCP8.5	Median	16	14	-1	8	9
2041–2070	RCP8.5	95 %	32	25	21	23	20
2071–2100	RCP2.6	5 %	-3	-3	-11	-5	-2
2071–2100	RCP2.6	Median	9	7	3	6	6
2071–2100	RCP2.6	95 %	21	17	17	17	15
2071–2100	RCP4.5	5 %	3	0	-14	-5	1
2071–2100	RCP4.5	Median	16	14	4	9	11
2071–2100	RCP4.5	95 %	30	28	22	23	20
2071–2100	RCP8.5	5 %	7	6	-32	-3	0
2071–2100	RCP8.5	Median	28	19	-1	14	15
2071–2100	RCP8.5	95 %	50	33	30	32	30

Table 5. Projected seasonal and annual mean changes in daily minimum temperatures (in °C) for Latvia; for further information, see the caption of Table 3.

Period	Forcing	Quantile	DJF	MAM	JJA	SON	ANN
2011–2040	RCP2.6	5 %	0.5	0.5	0.6	0.5	0.7
2011–2040	RCP2.6	Median	2.0	1.6	1.3	1.3	1.6
2011–2040	RCP2.6	95 %	3.6	2.6	2.1	2.1	2.4
2011–2040	RCP4.5	5 %	0.5	0.6	0.6	0.5	0.8
2011–2040	RCP4.5	Median	2.2	1.6	1.4	1.4	1.7
2011–2040	RCP4.5	95 %	4.0	2.7	2.1	2.3	2.6
2011–2040	RCP8.5	5 %	0.6	0.7	0.6	0.7	0.9
2011–2040	RCP8.5	Median	2.3	1.7	1.5	1.5	1.7
2011–2040	RCP8.5	95 %	4.0	2.7	2.4	2.3	2.6
2041–2070	RCP2.6	5 %	1.1	0.8	0.6	0.8	1.0
2041–2070	RCP2.6	Median	2.6	2.1	1.7	1.8	2.0
2041–2070	RCP2.6	95 %	4.1	3.3	2.7	2.7	3.1
2041–2070	RCP4.5	5 %	1.3	1.1	1.0	1.1	1.3
2041–2070	RCP4.5	Median	3.4	2.6	2.1	2.3	2.6
2041–2070	RCP4.5	95 %	5.5	4.1	3.3	3.4	3.9
2041–2070	RCP8.5	5 %	2.7	1.8	1.5	1.9	2.2
2041–2070	RCP8.5	Median	4.6	3.3	2.9	3.2	3.5
2041–2070	RCP8.5	95 %	6.4	4.8	4.4	4.5	4.8
2071–2100	RCP2.6	5 %	1.1	0.6	0.5	0.8	0.9
2071–2100	RCP2.6	Median	2.6	1.9	1.7	1.8	2.0
2071–2100	RCP2.6	95 %	4.1	3.3	2.9	2.8	3.1
2071–2100	RCP4.5	5 %	2.1	1.5	1.2	1.4	1.7
2071–2100	RCP4.5	Median	4.3	3.2	2.6	2.9	3.2
2071–2100	RCP4.5	95 %	6.5	4.8	4.0	4.4	4.7
2071–2100	RCP8.5	5 %	4.0	2.9	2.4	2.9	3.4
2071–2100	RCP8.5	Median	6.7	5.0	4.6	4.9	5.3
2071–2100	RCP8.5	95 %	9.5	7.1	6.9	6.8	7.2

Table 6. Projected seasonal and annual mean changes in daily maximum temperatures (in °C) for Latvia; for further information, see the caption of Table 3.

Period	Forcing	Quantile	DJF	MAM	JJA	SON	ANN
2011–2040	RCP2.6	5 %	0.3	0.3	0.3	0.5	0.6
2011–2040	RCP2.6	Median	1.6	1.5	1.5	1.4	1.5
2011–2040	RCP2.6	95 %	2.9	2.7	2.7	2.3	2.4
2011–2040	RCP4.5	5 %	0.3	0.5	0.2	0.5	0.6
2011–2040	RCP4.5	Median	1.8	1.6	1.6	1.5	1.6
2011–2040	RCP4.5	95 %	3.2	2.8	2.9	2.5	2.6
2011–2040	RCP8.5	5 %	0.5	0.5	0.2	0.6	0.8
2011–2040	RCP8.5	Median	1.8	1.6	1.6	1.6	1.6
2011–2040	RCP8.5	95 %	3.2	2.7	2.9	2.5	2.5
2041–2070	RCP2.6	5 %	0.9	0.5	0.4	0.7	0.8
2041–2070	RCP2.6	Median	2.1	2.0	1.8	1.9	1.9
2041–2070	RCP2.6	95 %	3.3	3.5	3.3	3.0	3.1
2041–2070	RCP4.5	5 %	1.0	0.9	0.7	1.1	1.2
2041–2070	RCP4.5	Median	2.7	2.5	2.4	2.4	2.5
2041–2070	RCP4.5	95 %	4.4	4.1	4.1	3.6	3.8
2041–2070	RCP8.5	5 %	2.1	1.3	1.0	1.9	1.8
2041–2070	RCP8.5	Median	3.7	3.0	3.2	3.3	3.3
2041–2070	RCP8.5	95 %	5.3	4.8	5.4	4.7	4.8
2071–2100	RCP2.6	5 %	0.9	0.4	0.3	0.7	0.7
2071–2100	RCP2.6	Median	2.1	1.9	1.8	1.9	1.9
2071–2100	RCP2.6	95 %	3.3	3.4	3.4	3.0	3.1
2071–2100	RCP4.5	5 %	1.8	1.4	0.9	1.4	1.6
2071–2100	RCP4.5	Median	3.4	3.0	2.9	3.0	3.1
2071–2100	RCP4.5	95 %	5.1	4.6	4.8	4.6	4.5
2071–2100	RCP8.5	5 %	3.4	2.5	1.8	2.8	2.9
2071–2100	RCP8.5	Median	5.6	4.7	5.0	5.0	5.1
2071–2100	RCP8.5	95 %	7.7	6.9	8.2	7.2	7.2

Table 7. Projected seasonal and annual mean changes in the difference between daily maximum and minimum temperatures (in %) for Latvia; for further information, see the caption of Table 3.

Period	Forcing	Quantile	DJF	MAM	JJA	SON	ANN
2011–2040	RCP2.6	5 %	-18	-8	-6	-7	-7
2011–2040	RCP2.6	Median	-9	-1	2	2	-1
2011–2040	RCP2.6	95 %	0	6	10	10	5
2011–2040	RCP4.5	5 %	-20	-9	-7	-9	-9
2011–2040	RCP4.5	Median	-10	0	3	2	-1
2011–2040	RCP4.5	95 %	0	8	13	14	7
2011–2040	RCP8.5	5 %	-20	-9	-7	-7	-8
2011–2040	RCP8.5	Median	-10	-1	1	1	-1
2011–2040	RCP8.5	95 %	0	6	10	10	5
2041–2070	RCP2.6	5 %	-22	-10	-6	-7	-9
2041–2070	RCP2.6	Median	-11	-1	2	2	-1
2041–2070	RCP2.6	95 %	0	8	10	11	6
2041–2070	RCP4.5	5 %	-28	-12	-8	-11	-12
2041–2070	RCP4.5	Median	-15	-1	4	3	-1
2041–2070	RCP4.5	95 %	-1	11	15	16	9
2041–2070	RCP8.5	5 %	-34	-15	-9	-10	-14
2041–2070	RCP8.5	Median	-19	-3	3	2	-3
2041–2070	RCP8.5	95 %	-4	9	16	15	8
2071–2100	RCP2.6	5 %	-21	-9	-5	-6	-8
2071–2100	RCP2.6	Median	-11	-1	2	2	-1
2071–2100	RCP2.6	95 %	-2	7	8	10	5
2071–2100	RCP4.5	5 %	-35	-16	-10	-13	-15
2071–2100	RCP4.5	Median	-19	-2	3	2	-3
2071–2100	RCP4.5	95 %	-2	12	16	18	10
2071–2100	RCP8.5	5 %	-46	-20	-13	-15	-19
2071–2100	RCP8.5	Median	-25	-4	4	3	-4
2071–2100	RCP8.5	95 %	-4	13	21	20	11

Table 8. Projected seasonal and annual mean changes in surface wind speed (in %) for Latvia; for further information, see the caption of Table 3.

Period	Forcing	Quantile	DJF	MAM	JJA	SON	ANN
2011–2040	RCP2.6	5 %	-5	-6	-4	-5	-4
2011–2040	RCP2.6	Median	0	0	0	-1	0
2011–2040	RCP2.6	95 %	5	6	3	3	3
2011–2040	RCP4.5	5 %	-8	-10	-7	-9	-7
2011–2040	RCP4.5	Median	-2	-2	-2	-3	-2
2011–2040	RCP4.5	95 %	4	5	3	3	3
2011–2040	RCP8.5	5 %	-7	-8	-4	-6	-6
2011–2040	RCP8.5	Median	1	0	1	0	0
2011–2040	RCP8.5	95 %	9	8	5	6	6
2041–2070	RCP2.6	5 %	-13	-12	-4	-7	-8
2041–2070	RCP2.6	Median	-2	-1	0	-1	-1
2041–2070	RCP2.6	95 %	9	9	5	6	6
2041–2070	RCP4.5	5 %	-19	-17	-11	-13	-13
2041–2070	RCP4.5	Median	-4	-4	-3	-4	-4
2041–2070	RCP4.5	95 %	11	8	5	5	6
2041–2070	RCP8.5	5 %	-18	-15	-6	-9	-11
2041–2070	RCP8.5	Median	0	0	1	0	0
2041–2070	RCP8.5	95 %	17	14	7	8	11
2071–2100	RCP2.6	5 %	-23	-17	-4	-9	-13
2071–2100	RCP2.6	Median	-2	-2	0	-1	-1
2071–2100	RCP2.6	95 %	18	13	5	7	10
2071–2100	RCP4.5	5 %	-27	-22	-12	-16	-18
2071–2100	RCP4.5	Median	-5	-6	-3	-4	-5
2071–2100	RCP4.5	95 %	17	10	7	7	8
2071–2100	RCP8.5	5 %	-27	-20	-7	-12	-16
2071–2100	RCP8.5	Median	-1	-1	0	-1	-1
2071–2100	RCP8.5	95 %	25	17	7	10	14

Table 9. Projected seasonal changes (means of parallel runs) in four climate variables from 1971–2000 to 2070–2099 under the RCP2.6 scenario as simulated by the individual GCMs; spatial averages over Latvia. DJF: December to February; MAM: March to May; JJA: June to August; SON: September to November.

Model	Temperature (^{o}C)				Precipitation (%)				Temp. range (^{o}C)				Wind speed (%)			
	DJF	MAM	JJA	SON	DJF	MAM	JJA	SON	DJF	MAM	JJA	SON	DJF	MAM	JJA	SON
MIROC5	2.5	3.9	3.1	2.3	8	8	-7	16	-0.4	0.9	0.8	0.6	-3	1	3	0
MIROC-ESM	3.3	3.6	3.0	3.1	36	15	9	26	-0.4	-0.0	0.1	0.0	-62	-57	1	-45
MIROC-ESM-CHEM	3.2	3.5	2.8	2.9	30	20	12	25	-0.5	-0.0	0.1	-0.1	-57	-57	3	-39
MRI-CGCM3	2.3	1.8	1.0	1.3	3	8	15	4	-1.1	-0.6	-0.2	-0.1	-2	-4	2	1
BCC-CSM1-1	2.2	1.9	1.5	2.0	5	-3	6	7	-0.9	-0.0	0.2	0.2	-1	1	0	1
INMCM4	–	–	–	–	–	–	–	–	–	–	–	–	–	–	–	–
NorESM1-M	1.8	1.7	2.2	1.9	6	3	8	5	-0.3	0.4	0.3	0.2	–	–	–	–
NorESM1-ME	2.3	2.5	1.8	2.3	8	8	-2	10	–	–	–	–	–	–	–	–
HadGEM2-ES	3.3	2.6	2.5	2.3	10	3	-3	1	-0.6	0.1	0.1	0.3	-1	-2	0	-1
HadGEM2-CC	–	–	–	–	–	–	–	–	–	–	–	–	–	–	–	–
MPI-ESM-LR	1.7	1.6	0.7	1.3	4	7	4	1	-0.3	-0.2	-0.1	-0.0	0	-3	1	0
MPI-ESM-MR	2.7	1.3	0.8	1.1	17	14	-5	2	-0.6	-0.4	-0.0	-0.1	1	0	2	1
CNRM-CM5	2.6	1.6	1.8	1.9	9	16	1	-1	-0.5	-0.2	-0.1	0.3	0	1	6	-1
IPSL-CM5A-LR	4.0	2.6	2.5	2.1	17	0	13	10	–	–	–	–	3	-1	-2	-2
IPSL-CM5A-MR	2.2	1.8	1.6	2.1	4	8	6	4	–	–	–	–	-1	-1	0	-2
CMCC-CM	–	–	–	–	–	–	–	–	–	–	–	–	–	–	–	–
CMCC-CMS	–	–	–	–	–	–	–	–	–	–	–	–	–	–	–	–
GFDL-CM3	3.5	2.8	3.4	2.9	13	12	13	9	-0.6	-0.0	0.5	0.5	2	3	1	1
GFDL-ESM2M	2.9	1.5	0.8	1.8	18	10	18	15	–	–	–	–	2	-1	0	-2
GISS-E2-R	1.0	0.4	0.8	0.7	0	0	2	2	-0.3	0.1	0.1	0.1	3	2	1	2
GISS-E2-H	1.3	0.9	1.5	1.5	-3	-5	-4	2	-0.4	0.0	0.1	0.0	-2	-2	-1	-1
NCAR-CCSM4	1.5	1.3	1.6	1.3	5	5	1	8	-0.4	-0.0	0.2	-0.0	–	–	–	–
NCAR-CESM1-CAM5	1.8	2.1	2.5	1.9	17	20	10	9	-0.2	0.4	0.4	0.4	3	3	3	0
NCAR-CESM1-BGC	–	–	–	–	–	–	–	–	–	–	–	–	–	–	–	–
CanESM2	3.0	2.7	2.6	2.5	10	18	7	11	-0.9	-0.4	0.2	-0.2	-2	1	-6	-4
ACCESS1-0	–	–	–	–	–	–	–	–	–	–	–	–	–	–	–	–
ACCESS1-3	–	–	–	–	–	–	–	–	–	–	–	–	–	–	–	–
EC-EARTH	1.5	1.6	1.2	1.1	7	9	16	2	-0.4	-0.3	-0.3	-0.1	0	-1	0	-5

Table 10. As in Table 9 but for the RCP4.5 scenario.

Model	Temperature (°C)				Precipitation (%)				Temp. range (°C)				Wind speed (%)			
	DJF	MAM	JJA	SON	DJF	MAM	JJA	SON	DJF	MAM	JJA	SON	DJF	MAM	JJA	SON
MIROC5	3.4	4.8	3.4	3.6	9	15	4	16	-0.7	0.9	0.7	0.6	-7	-5	-13	-6
MIROC-ESM	4.2	4.5	4.0	3.8	40	28	5	33	-0.7	-0.7	0.2	-0.2	-67	-61	0	-46
MIROC-ESM-CHEM	4.5	4.3	3.7	4.4	47	20	40	33	-0.7	-0.4	-0.1	-0.3	-65	-64	1	-45
MRI-CGCM3	3.6	2.0	1.5	2.2	10	15	19	8	-1.6	-0.8	-0.3	-0.3	-3	-4	2	2
BCC-CSM1-1	3.9	3.1	2.4	3.0	16	5	1	9	-1.2	-0.4	0.4	0.2	1	0	2	2
INMCM4	3.6	1.5	0.7	1.2	9	-2	14	12	-1.2	-0.3	-1.0	-0.7	3	-1	3	2
NorESM1-M	3.5	2.8	2.9	2.9	12	12	-3	14	-0.6	0.8	1.1	0.5	–	–	–	–
NorESM1-ME	3.2	3.7	2.7	2.7	17	9	-4	17	–	–	–	–	–	–	–	–
HadGEM2-ES	4.1	3.8	4.0	3.8	16	11	-8	5	-0.8	0.0	0.1	0.3	-8	-12	-7	-8
HadGEM2-CC	5.1	4.0	3.6	4.0	16	24	-4	0	-1.4	-0.2	-0.1	0.3	-10	-7	-5	-8
MPI-ESM-LR	2.7	2.1	1.5	2.0	9	11	3	8	-0.5	-0.3	-0.1	-0.2	-4	-8	-4	-5
MPI-ESM-MR	3.7	2.2	1.7	1.7	23	15	3	2	-0.8	-0.4	0.0	-0.2	-3	-6	-5	-8
CNRM-CM5	4.4	3.9	2.9	3.0	17	27	5	8	-0.8	-0.5	-0.2	-0.1	0	-3	3	-2
IPSL-CM5A-LR	5.4	4.0	3.5	3.6	24	3	26	13	–	–	–	–	-1	-5	-7	-5
IPSL-CM5A-MR	4.6	2.8	2.9	3.6	19	-3	4	3	–	–	–	–	-1	-5	-4	-5
CMCC-CM	7.0	4.3	2.4	4.6	31	18	1	-4	-2.2	-1.3	-0.3	-0.4	2	0	6	3
CMCC-CMS	5.1	3.5	3.1	4.2	16	15	9	8	-1.4	-0.7	0.1	-0.3	-2	0	0	0
GFDL-CM3	4.7	4.2	4.2	3.8	30	27	5	18	-0.6	-0.0	0.8	0.4	2	-3	-7	-2
GFDL-ESM2M	3.2	1.7	1.0	2.5	20	14	22	9	-0.5	-0.0	-0.1	0.3	-4	-8	-7	-8
GISS-E2-R	3.8	2.3	2.1	2.1	11	10	11	5	-0.9	-0.4	-0.1	-0.2	-3	-4	-5	-3
GISS-E2-H	4.0	3.1	2.8	3.0	10	11	1	9	-1.0	-0.4	-0.1	-0.3	-8	-7	-7	-7
NCAR-CCSM4	1.8	1.9	2.6	2.0	10	9	-2	5	-0.4	0.5	1.2	0.5	–	–	–	–
NCAR-CESM1-CAM5	2.8	3.0	3.3	2.8	24	17	3	12	-0.2	1.1	1.5	1.1	-2	-2	-1	-4
NCAR-CESM1-BGC	2.1	2.3	2.6	1.7	13	12	-2	5	-0.4	0.8	1.1	0.7	–	–	–	–
CanESM2	4.2	3.3	3.7	3.4	21	27	3	10	-1.1	-0.5	0.4	-0.1	-9	-7	-14	-16
ACCESS1-0	3.3	2.7	3.6	3.1	7	24	-19	-6	-0.6	0.1	1.0	0.8	1	0	2	2
ACCESS1-3	3.4	3.1	4.0	2.8	14	19	-6	9	-0.3	0.8	1.4	0.9	4	1	0	3
EC-EARTH	2.4	2.7	2.1	2.4	8	14	9	7	-0.6	-0.5	-0.3	-0.2	-4	-4	-2	-3

Table 11. As in Table 9 but for the RCP8.5 scenario.

Model	Temperature (°C)				Precipitation (%)				Temp. range (°C)				Wind speed (%)			
	DJF	MAM	JJA	SON	DJF	MAM	JJA	SON	DJF	MAM	JJA	SON	DJF	MAM	JJA	SON
MIROC5	6.2	7.3	5.6	5.7	19	17	2	23	-1.0	0.9	0.6	0.5	-7	-2	-6	-4
MIROC-ESM	6.6	6.6	6.4	6.2	76	45	16	48	-0.6	-0.7	-0.3	-0.3	-69	-64	2	-48
MIROC-ESM-CHEM	7.2	6.6	6.2	6.5	63	29	30	47	-0.7	-0.4	-0.3	-0.4	-66	-66	2	-50
MRI-CGCM3	5.5	3.6	3.3	3.9	18	23	33	8	-2.0	-1.0	-0.5	-0.3	-5	-5	2	0
BCC-CSM1-1	6.6	4.6	3.9	4.1	31	16	-6	14	-1.7	-0.6	0.3	0.1	3	2	2	1
INMCM4	4.9	2.7	1.8	2.4	19	17	12	18	-1.4	-1.7	-1.2	-0.9	2	2	3	0
NorESM1-M	5.1	4.0	5.7	4.4	17	8	-15	23	-0.9	0.7	0.9	0.3	–	–	–	–
NorESM1-ME	5.4	4.6	5.1	4.2	33	15	-10	19	–	–	–	–	–	–	–	–
HadGEM2-ES	6.4	5.8	7.2	6.5	25	16	-33	-1	-1.0	0.0	0.6	0.7	-4	-6	-2	-5
HadGEM2-CC	7.6	6.2	6.6	6.6	22	26	-25	9	-1.8	-0.3	0.3	0.5	-7	-5	-1	-2
MPI-ESM-LR	4.7	3.7	3.0	4.0	22	20	3	13	-0.8	-0.5	-0.1	-0.1	1	-2	2	1
MPI-ESM-MR	5.8	3.3	3.0	3.8	28	30	-5	0	-1.0	-0.6	0.1	-0.1	3	1	1	-2
CNRM-CM5	5.8	4.6	3.9	4.0	19	30	25	18	-1.1	-0.9	-0.9	-0.3	0	-1	1	0
IPSL-CM5A-LR	8.7	6.3	6.2	6.2	39	7	28	20	–	–	–	–	6	1	-7	-4
IPSL-CM5A-MR	6.7	4.3	5.0	5.6	34	18	14	25	–	–	–	–	8	3	-4	1
CMCC-CM	9.3	6.6	4.1	6.7	40	21	-4	8	-2.7	-1.4	-0.2	-0.5	0	3	4	3
CMCC-CMS	9.5	5.4	4.5	6.3	37	16	-3	14	-2.2	-0.9	0.1	-0.3	0	0	0	2
GFDL-CM3	7.4	6.1	7.0	6.4	49	27	-3	20	-0.4	0.3	0.9	0.6	24	14	5	13
GFDL-ESM2M	5.5	3.7	2.5	4.1	35	9	21	17	-0.7	0.1	-0.1	0.4	13	8	6	6
GISS-E2-R	6.8	4.3	3.5	3.9	22	22	16	6	-1.6	-0.6	0.1	-0.2	1	2	-1	1
GISS-E2-H	6.6	5.0	4.4	4.8	12	10	6	12	-1.4	-0.2	0.0	-0.3	-4	-2	-5	-3
NCAR-CCSM4	3.9	3.2	4.6	3.7	20	14	-14	10	-0.8	0.3	0.9	0.3	–	–	–	–
NCAR-CESM1-CAM5	5.1	4.2	5.7	5.1	42	27	-16	18	-0.6	0.7	1.1	0.7	6	5	4	1
NCAR-CESM1-BGC	4.3	3.9	4.4	3.5	14	17	-18	-1	-0.9	0.7	1.2	0.7	–	–	–	–
CanESM2	6.0	5.2	6.9	5.8	33	34	-15	10	-1.4	-0.5	1.3	0.4	1	3	-9	-7
ACCESS1-0	5.9	5.3	7.3	5.4	15	10	-45	2	-0.7	0.4	2.1	1.1	3	1	3	5
ACCESS1-3	5.2	4.4	6.5	4.8	32	23	-14	20	-0.2	0.8	1.8	1.0	5	3	-1	3
EC-EARTH	4.0	4.1	3.5	4.0	15	22	11	9	-0.8	-0.6	-0.4	-0.1	-4	-1	2	-4

ILMATIETEEN LAITOS
METEOROLOGISKA INSTITUTET
FINNISH METEOROLOGICAL INSTITUTE

FINNISH METEOROLOGICAL INSTITUTE
Erik Palménin aukio 1
FIN-00560 Helsinki
tel. +358 29 539 1000
WWW.FMI.FI

ILMATIETEEN LAITOS
REPORTS 2016:7
ISBN 978-952-336-003-7 (pdf)
ISSN 0782-6079
Helsinki 2016